arXiv:1611.00168v2 [hep-ph] 23 Dec 2016

A chiral covariant approach to $\rho\rho$ scattering

D. Gülmez[a], U.-G. Meißner[a,b], J. A. Oller[c]

[a] *Helmholtz-Institut für Strahlen- und Kernphysik and Bethe Center for Theoretical Physics, Universität Bonn, D–53115 Bonn, Germany*

[b] *Institute for Advanced Simulation, Institut für Kernphysik and Jülich Center for Hadron Physics, Forschungszentrum Jülich, D-52425 Jülich, Germany*

[c] *Departamento de Física, Universidad de Murcia, E-30071 Murcia, Spain*

Abstract

We analyze vector meson – vector meson scattering in a unitarized chiral theory based on a chiral covariant framework. We show that a pole assigned to the scalar meson $f_0(1370)$ can be dynamically generated from the $\rho\rho$ interaction, while this is not the case for the tensor meson $f_2(1270)$ as found in earlier works. We show that the generation of the tensor state is untenable due to the extreme non-relativistic kinematics used before. We further consider the effects arising from the coupling of channels with different orbital angular momenta which are also important. We suggest to use the formalism outlined here to obtain more reliable results for the dynamical generation of resonances in the vector-vector interaction.

1 Introduction

It is now commonly accepted that some hadron resonances are generated by strong non-perturbative hadron-hadron interactions. Arguably the most famous example is the $\Lambda(1405)$, that arises from the coupled-channel dynamics of the strangeness $S = -1$ ground state octet meson-baryon channels in the vicinity of the $\pi\Sigma$ and K^-p thresholds [1]. This resonance also has the outstanding feature of being actually the combination of two near poles, the so-called two-pole nature of the $\Lambda(1405)$. In a field-theoretic sense, one should consider this state as two particles. This fact was predicted theoretically [2,3] and later unveiled experimentally [4] (see also the discussion in Ref. [5]). Another example is the scalar meson $f_0(980)$ close to the $\bar{K}K$ threshold, that is often considered to arise due to the strong S-wave interactions in the $\pi\pi$-$\bar{K}K$ system with isospin zero [6–8]. A new twist was given to this field in Ref. [9] where the S-wave vector-vector ($\rho\rho$) interactions were investigated and it was found that due to the strong binding in certain channels, the $f_2(1270)$ and the $f_0(1370)$ mesons could be explained as $\rho\rho$ bound states. This approach offered also an explanation why the tensor state f_2 is lighter than the scalar one f_0, as the leading order attraction in the corresponding $\rho\rho$ channel is stronger. This work was followed up by extensions to SU(3) [10], to account for radiative decays [11] and many other works, see e.g the short review in Ref. [12].

These results are certainly surprising and at odds with well-known features of the strong interactions. In this respect it is a text-book result that the $f_2(1270)$ fits very well within a nearly ideally-mixed P-wave $q\bar{q}$ nonet comprising as well the $a_2(1320)$, $f_2'(1525)$ and $K_s^*(1430)$ resonances [13–16]. Values for this mixing angle can be obtained from either the linear or quadratic mass relations as in Ref. [16]. Non-relativistic quark model calculations [17], as well as with relativistic corrections [18], predict that the coupling of the tensor mesons to $\gamma\gamma$ should be predominantly through helicity two by an $E1$ transition.

This simple $q\bar{q}$ picture for the tensor $f_2(1270)$ resonance has been recently validated by the analyses performed in Ref. [19] of the high-statistics Belle data [20, 21] on $\gamma\gamma \to \pi\pi$ in both the neutral and charged pion channels. Another point of importance in support of the $q\bar{q}$ nature of the $f_2(1270)$ is Regge theory, since this resonance lays in a parallel linear exchange-degenerate Regge trajectory with a "universal" slope parameter of around 1 GeV [22, 23]. Masses and widths of the first resonances with increasing spin laying on this Regge trajectory (ρ, f_2, ρ_3, f_4) are nicely predicted [24] by the dual-hadronic model of Lovelace-Shapiro-Veneziano [25].

One should stress that the results of Ref. [9] were obtained based on extreme non-relativistic kinematics, $\mathbf{p}_i^2/m_\rho^2 \simeq 0$, with $\mathbf{p}$ the rho-meson three-momentum and m_ρ the vector meson mass. This approximation, however, leads to some severe simplifications:

- Due to the assumed threshold kinematics, the full ρ propagator was reduced to its scalar form, thus enabling the use of techniques already familiar from the pion-pion interaction [8]. This was applied when considering the iteration of the interactions in the Bethe-Salpeter equation.
- Based on the same argument, the algebra involving the spin and the isospin projectors of the two vector-meson states could considerably be simplified.

However, as $\sqrt{s_{\rm th}} = 2m_\rho = 1540$ MeV, the lighter of the bound states is already quite far away from the 2ρ threshold. It is therefore legitimate to question the assumptions made in Ref. [9]. In this work, we will reanalyze the same reactions using a fully covariant approach. This is technically much more involved than the formalism of the earlier works. However, as our aim is to scrutinize the approximations made there, we stay as much as possible close to their choice of parameters. Additionally, we also consider coupled-channel scattering including channels with nonzero orbital angular momentum, that is, we go beyond the S-wave scattering approximation of Ref. [9]. The inclusion of coupled channels is also important when moving away from threshold. The authors of this reference only considered scattering in S-wave because of the same type of near-threshold arguments. As will be shown, the near-threshold approximation is only reliable very close to threshold.

Our work is organized as follows: In Sec. 2 we outline the formalism to analyze $\rho\rho$ scattering in a covariant fashion. In particular, we retain the full propagator structure of the ρ, which leads to a very different analytic structure of the scattering amplitude compared to the extreme non-relativistic framework. We also perform a partial-wave projection technique, that allows to perform the unitarization of the tree-level scattering amplitudes using methods well established in the literature. An elaborate presentation of our results is given in Sec. 3, where we also give a detailed comparison to the earlier work based on the non-relativistic framework. Next, we consider the effect of the coupling between channels with different orbital angular momentum. We also improve the unitarization procedure by considering the first-iterated solution of the N/D method in Sec. 4, reinforcing our results obtained with the simpler unitarization method. We conclude with a summary and discussion in Sec. 5. A detailed account of the underlying projection formalism is given in App. A.

2 Formalism

The inclusion of vector mesons in a chiral effective Lagrangian can be done in a variety of different ways, such as treating them as heavy gauge bosons, using a tensor field formulation or generating them as hidden gauge particles of the non-linear σ-model. All these approaches are equivalent, as shown e.g. in the review [26]. While in principle the tensor field formulation is preferable in the construction of chiral-invariant building blocks, we stick here to the hidden symmetry approach as this was also used in Ref. [9].

To be specific, the Lagrangian for the interactions among vector mesons is taken from the pure gauge-boson part of the non-linear chiral Lagrangian with hidden local symmetry [27, 28],

$$\mathcal{L}' = -\frac{1}{4}\langle F_{\mu\nu}F^{\mu\nu}\rangle \ . \tag{1}$$

Here, the symbol $\langle\ldots\rangle$ denotes the trace in SU(2) flavor space and the field strength tensor $F_{\mu\nu}$ is

$$F_{\mu\nu} = \partial_\mu V_\nu - \partial_\nu V_\mu - ig[V_\mu, V_\nu] \ , \tag{2}$$

with the coupling constant $g = M_V/2f_\pi$ and $f_\pi \approx 92$ MeV [5] the weak pion decay constant. The vector field V_μ is

$$V_\mu = \begin{pmatrix} \frac{1}{\sqrt{2}}\rho^0 & \rho^+ \\ \rho^- & -\frac{1}{\sqrt{2}}\rho^0 \end{pmatrix} \tag{3}$$

From the Lagrangian in Eq. (1) one can straightforwardly derive the interaction between three and four vector mesons and the corresponding vertices. The corresponding Lagrangians are denoted as $\mathcal{L}'_3$ and $\mathcal{L}'_4$, respectively. The former one gives rise to $\rho\rho$ interactions through the exchange of a ρ meson and the latter corresponds to purely contact interactions. We did not include the ω resonance in Eq. (3) since it does not contribute to the interaction part (in the isospin limit).

Consider first the contact vertices for the 4ρ interaction. These can be derived from Eq. (2) by keeping the terms proportional to g^2, leading to

$$\mathcal{L}'_4 = \frac{g^2}{2}\langle V_\mu V_\nu V^\mu V^\nu - V_\mu V^\mu V_\nu V^\nu\rangle \ . \tag{4}$$

The three different isospin (I) amplitudes for $\rho\rho$ scattering ($I = 0$, 1 and 2) can be worked out from the knowledge of the transitions $\rho^+(p_1)\rho^-(p_2) \to \rho^+(p_3)\rho^-(p_4)$ and $\rho^+(p_1)\rho^-(p_2) \to \rho^0(p_3)\rho^0(p_4)$ by invoking crossing as well. We have indicated the different four-momenta by p_i, $i = 1, \ldots, 4$. The scattering amplitude for the former transition is denoted by $A(p_1, p_2, p_3, p_4)$ and the latter one by $B(p_1, p_2, p_3, p_4)$, which are shown in Figs. 1 and 2, respectively.

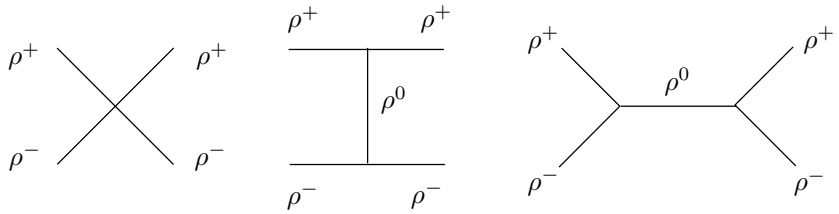


Figure 1: Feynman diagrams for the tree-level amplitude $\rho^+\rho^- \to \rho^+\rho^-$.

The contributions to those amplitudes from $\mathcal{L}'_4$, cf. Eq. (4), are indicated by the subscript c and are given by:

$$\begin{aligned} A_c(k_1, k_2, k_3, k_4) =& -2g^2(2\epsilon(1)_\mu\epsilon(2)_\nu\epsilon(3)^\nu\epsilon(4)^\mu - \epsilon(1)_\mu\epsilon(2)^\mu\epsilon(3)_\nu\epsilon(4)^\nu - \epsilon(1)_\mu\epsilon(2)_\nu\epsilon(3)^\mu\epsilon(4)^\nu) \ , \\ B_c(k_1, k_2, k_3, k_4) =& 2g^2(2\epsilon(1)_\mu\epsilon(2)^\mu\epsilon(3)_\nu\epsilon(4)^\nu - \epsilon(1)_\mu\epsilon(2)_\nu\epsilon(3)^\mu\epsilon(4)^\nu - \epsilon(1)_\mu\epsilon(2)_\nu\epsilon(3)^\nu\epsilon(4)^\mu) \ . \end{aligned} \tag{5}$$

In this equation, the $\epsilon(i)_\mu$ corresponds to the polarization vector of the i^{th} ρ. Each polarization vector is characterized by its three-momentum $\mathbf{p}_i$ and third component of the spin σ_i in its rest frame, so that

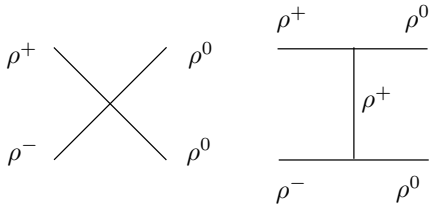


Figure 2: Feynman diagrams for the tree-level amplitude $\rho^+\rho^- \to \rho^0\rho^0$.

$\epsilon(i)_\mu \equiv \epsilon(\mathbf{p}_i, \sigma_i)_\mu$. Explicit expressions of these polarization vectors are given in Eqs. (A.9) and (A.10) of Appendix A. In the following, so as to simplify the presentation, the tree-level scattering amplitudes are written for real polarization vectors. The same expressions are valid for complex ones by taking the complex conjugate of the polarization vectors attached to the final particles.[1]

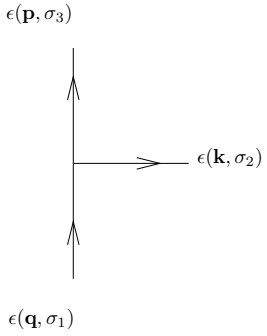


Figure 3: Three-ρ vertex from $\mathcal{L}_3'$.

Considering the one-vector exchange terms, we need the three-vector interaction Lagrangian $\mathcal{L}_3'$. It reads

$$\mathcal{L}_3' = ig\langle(\partial_\mu V_\nu - \partial_\nu V_\mu)V^\mu V^\nu\rangle \ . \tag{6}$$

The basic vertex is depicted in Fig. 3 which after a simple calculation can be written as

$$\begin{aligned} V_3 = &-\sqrt{2}g\Big[(q_\mu\epsilon(1)_\nu - q_\nu\epsilon(1)_\mu)\epsilon(3)^\mu\epsilon(2)^\nu - (k_\mu\epsilon(2)_\nu - k_\nu\epsilon(2)_\mu)\epsilon(1)^\mu\epsilon(3)^\nu \\ &- (p_\mu\epsilon(3)_\nu - p_\nu\epsilon(3)_\mu)\epsilon(2)^\mu\epsilon(1)^\nu\Big] \ . \end{aligned} \tag{7}$$

In terms of this vertex, one can straightforwardly calculate the vector exchange diagrams in Figs. 1 and 2. The expression for the t-channel ρ-exchange amplitude, the middle diagram in Fig. 1, and denoted by

[1]The polarization vectors $\epsilon(\mathbf{p}, \sigma)$ in the Appendix A are complex, so that the polarization vectors associated with the final-state $\rho\rho$ should be complex conjugated in this case.

$A_t(p_1,p_2,p_3,p_4;\epsilon_1,\epsilon_2,\epsilon_3,\epsilon_4)$, is

$$A_t(p_1,p_2,p_3,p_4;\epsilon_1,\epsilon_2,\epsilon_3,\epsilon_4) = \frac{2g^2}{(p_1-p_3)^2-m_\rho^2+i0^+}\big[(p_1(p_2+p_4)+p_3(p_2+p_4))\epsilon_1\cdot\epsilon_3\epsilon_2\cdot\epsilon_4$$
$$+4(\epsilon_1\cdot k_3\epsilon_4\cdot k_2\epsilon_2\cdot\epsilon_3+\epsilon_1\cdot k_3\epsilon_2\cdot k_4\epsilon_3\cdot\epsilon_4+\epsilon_3\cdot k_1\epsilon_4\cdot k_2\epsilon_1\cdot\epsilon_2+\epsilon_2\cdot k_4\epsilon_3\cdot k_1\epsilon_1\cdot\epsilon_4)$$
$$-2(\epsilon_1\cdot k_3(\epsilon_3\cdot k_2+\epsilon_3\cdot k_4)\epsilon_2\cdot\epsilon_4+\epsilon_3\cdot k_1(\epsilon_1\cdot k_2+\epsilon_1\cdot k_4)\epsilon_2\cdot\epsilon_4+\epsilon_2\cdot k_4(\epsilon_4\cdot k_1+\epsilon_4\cdot k_3)\epsilon_1\cdot\epsilon_3$$
$$+\epsilon_4\cdot k_2(\epsilon_2\cdot k_1+\epsilon_2\cdot k_3)\epsilon_1\cdot\epsilon_3)\big]\ , \tag{8}$$

where for short, we have rewritten $\epsilon(i)\to\epsilon_i$, and the scalar products involving polarization vectors are indicated with a dot. The u-channel ρ-exchange amplitude $A_u(p_1,p_2,p_3,p_4;\epsilon_1,\epsilon_2,\epsilon_3,\epsilon_4)$ can be obtained from the expression of A_t by exchanging $p_3\leftrightarrow p_4$ and $\epsilon_3\leftrightarrow\epsilon_4$. In the exchange for the polarization vectors they always refer to the same arguments of three-momentum and spin, that is, $\epsilon(\mathbf{p}_3,\sigma_3)\leftrightarrow\epsilon(\mathbf{p}_4,\sigma_4)$. In this way,

$$A_u(p_1,p_2,p_3,p_4;\epsilon_1,\epsilon_2,\epsilon_3,\epsilon_4) = A_t(p_1,p_2,p_4,p_3;\epsilon_1,\epsilon_2,\epsilon_4,\epsilon_3)\ . \tag{9}$$

Notice that the second diagram in Fig. 2 is a sum of the t-channel and u-channel ρ-exchange diagrams.

The s-channel exchange amplitude (the last diagram in Fig. 1) can also be obtained from A_t by performing the exchange $p_2\leftrightarrow -p_3$ and $\epsilon_2\leftrightarrow\epsilon_3$, with the same remark as above for the exchange of polarization vectors. We then have:

$$A_s(p_1,p_2,p_3,p_4;\epsilon_1,\epsilon_2,\epsilon_3,\epsilon_4) = A_t(p_1,-p_3,-p_2,p_4;\epsilon_1,\epsilon_3,\epsilon_2,\epsilon_4)\ . \tag{10}$$

The total amplitudes for $\rho^+\rho^-\to\rho^+\rho^-$ and $\rho^+\rho^-\to\rho^0\rho^0$ are

$$\begin{aligned} A &= A_c + A_t + A_s\ , \\ B &= B_c + A_t + A_u\ , \end{aligned} \tag{11}$$

with the usual arguments $(p_1,p_2,p_3,p_4;\epsilon_1,\epsilon_2,\epsilon_3,\epsilon_4)$. By crossing we also obtain the amplitude for $\rho^+\rho^+\to\rho^+\rho^+$ [that we denote as $C(p_1,p_2,p_3,p_4;\epsilon_1,\epsilon_2,\epsilon_3,\epsilon_4)$] from the one for $\rho^+\rho^-\to\rho^+\rho^-$ by exchanging $p_2\leftrightarrow -p_4$ and $\epsilon_2\leftrightarrow\epsilon_4$, that is,

$$C(p_1,p_2,p_3,p_4;\epsilon_1,\epsilon_2,\epsilon_3,\epsilon_4) = A(p_1,-p_4,p_3,-p_2;\epsilon_1,\epsilon_4,\epsilon_3,\epsilon_2)\ . \tag{12}$$

The amplitude C is purely $I=2$, that we denote as $T^{(2)}$. The amplitude B is an admixture of the $I=0$, $T^{(0)}$, and $I=2$ amplitudes,

$$B = \frac{1}{3}(T^{(0)}-T^{(2)})\ , \tag{13}$$

from which we find that

$$T^{(0)} = 3B + C\ . \tag{14}$$

To isolate the $I=1$ amplitude, $T^{(1)}$, we take the $\rho^+\rho^-$ elastic amplitude A which obeys the following isospin decomposition

$$A = \frac{1}{6}T^{(2)} + \frac{1}{2}T^{(1)} + \frac{1}{3}T^{(0)}\ . \tag{15}$$

Taking into account Eqs. (14) we conclude that

$$T^{(1)} = 2A - 2B - C \ . \tag{16}$$

In terms of these amplitudes with well-defined isospin the expression in Eq. (A.48) for calculating the partial-wave amplitudes in the ℓSJI basis (states with well-defined total angular momentum J, total spin S, orbital angular momentum ℓ and isospin I), denoted as $T^{(JI)}_{\ell S;\bar{\ell}\bar{S}}(s)$ for the transition $(\bar{\ell}\bar{S}JI) \to (\ell SJI)$, simplifies to

$$T^{(JI)}_{\ell S;\bar{\ell}\bar{S}}(s) = \frac{Y^0_{\bar{\ell}}(\hat{\mathbf{z}})}{2(2J+1)} \sum_{\substack{\sigma_1,\,\sigma_2,\,\bar{\sigma}_1 \\ \bar{\sigma}_2,\,m}} \int d\hat{\mathbf{p}}''\, Y^m_\ell(\mathbf{p}'')^* \, (\sigma_1\sigma_2 M|s_1 s_2 S)(mM\bar{M}|\ell SJ)(\bar{\sigma}_1\bar{\sigma}_2\bar{M}|\bar{s}_1\bar{s}_2\bar{S})(0\bar{M}\bar{M}|\bar{\ell}\bar{S}J)$$
$$\times T^{(I)}(p_1,p_2,p_3,p_4;\epsilon_1,\epsilon_2,\epsilon_3,\epsilon_4) \ , \tag{17}$$

with s the usual Mandelstam variable, $\mathbf{p}_1 = |\mathbf{p}|\hat{\mathbf{z}}$, $\mathbf{p}_2 = -|\mathbf{p}|\hat{\mathbf{z}}$, $\mathbf{p}_3 = \mathbf{p}''$ and $\mathbf{p}_4 = -\mathbf{p}''$, $M = \sigma_1 + \sigma_2$ and $\bar{M} = \bar{\sigma}_1 + \bar{\sigma}_2$

The Mandelstam variables t and u for $\rho\rho$ scattering in the isospin limit are given by $t = -2\mathbf{p}^2(1-\cos\theta)$ and $u = -2\mathbf{p}^2(1+\cos\theta)$, with θ the polar angle of the final momentum. The denominator in A_t due to the ρ propagator, cf. Eq. (8), vanishes for $t = m_\rho^2$ and similarly the denominator in A_u for $u = m_\rho^2$. When performing the angular projection in Eq. (17) these poles give rise to a left-hand cut starting at the branch point $s = 3m_\rho^2$. This can be easily seen by considering the integration on $\cos\theta$ of the fraction $1/(t - m_\rho^2 + i\varepsilon)$, which gives the same result both for the t and the u channel exchange,

$$\frac{1}{2}\int_{-1}^{+1} d\cos\theta \frac{1}{-2\mathbf{p}^2(1-\cos\theta) - m_\rho^2 + i\varepsilon} = -\frac{1}{4\mathbf{p}^2}\log\left(\frac{4\mathbf{p}^2 + m_\rho^2}{m_\rho^2} + \frac{4\mathbf{p}^2}{m_\rho^4} i\varepsilon\right) \ , \tag{18}$$

with $\varepsilon \to 0^+$. The argument of the log becomes negative for $4\mathbf{p}^2 < -m_\rho^2$, which is equivalent to $s < 3m_\rho^2$. Because of the factor $\mathbf{p}^2\varepsilon$ the imaginary part of the argument of the log below the threshold is negative which implies that the proper value of the partial-wave amplitude on the physical axis below the branch point at $s = 3m_\rho^2$ is reached in the limit of vanishing negative imaginary part of s. The presence of this branch point and left-hand cut was not noticed in Ref. [9], where only the extreme non-relativistic reduction was considered, so that the ρ propagators in the ρ-exchange amplitudes collapsed to just a constant.

Once we have calculated the partial-wave projected tree-level amplitude we proceed to its unitarization making use of standard techniques within unitary chiral perturbation theory [2, 8, 29]. This is a resummation technique that restores unitarity and also allows to study the resonance region. It has been applied to many systems and resonances by now, e.g. in meson-meson, meson-baryon, nucleon-nucleon and WW systems. Among many others we list some pioneering works for these systems [2, 3, 8, 30–40]. In the last years this approach has been applied also to systems containing mesons and baryons made from heavy quarks, some references on this topic are [41–45].

The basic equation to obtain the final unitarized T matrix in the subspace of coupled channels ℓSJI, with the same JI, is [2]

$$T^{(JI)}(s) = \left[I - V^{(JI)}(s)\cdot G(s)\right]^{-1} \cdot V^{(JI)}(s) \ . \tag{19}$$

[2] In order to easier the comparison with Ref. [9] we take the same sign convention for matrices $V(s)$ and $T(s)$ as in that reference.

Here, $G(s)$ is a diagonal matrix made up by the two-point loop function $g(s)$ with $\rho\rho$ as intermediate states,

$$g(s) \to i \int \frac{d^4q}{(2\pi)^4} \frac{1}{(q^2 - m_\rho^2)((P-q)^2 - m_\rho^2)} \ , \tag{20}$$

where $P^2 = s$ and within our normalization, cf. Eq. (A.53), Im $g(s) = -|\mathbf{p}|/8\pi\sqrt{s}$. The loop function $g(s)$ is logarithmically divergent and it can be calculated once its value at a given reference point is subtracted. In this way, one can write down a once-subtracted dispersion relation for $g(s)$ whose result is[3]

$$g(s) = \frac{1}{(4\pi)^2} \left(a(\mu) + \log \frac{m_\rho^2}{\mu^2} + \sigma \left[\log(\sigma+1) - \log(\sigma-1) \right] \right) \ , \tag{21}$$

with

$$\sigma = \sqrt{1 - \frac{4m_\rho^2}{s}} \ , \tag{22}$$

and μ is a renormalization scale typically taken around m_ρ, such the sum $a(\mu) + \log m_\rho^2/\mu^2$ is independent of μ. The subtraction constant in Eq. (21) could depend on the quantum numbers ℓ, S and J, but not on I due to the isospin symmetry [3].

To compare with the results of Ref. [9], we also evaluate the function $g(s)$ introducing a three-momentum cutoff $q_{\rm max}$, the resulting $g(s)$ function is denoted by $g_c(s)$,

$$g_c(s) = \frac{1}{2\pi^2} \int_0^{q_{\rm max}} dq \frac{q^2}{w(s - 4w^2 + i\varepsilon)} \ , \tag{23}$$

with $w = \sqrt{q^2 + m_\rho^2}$. This integral can be done algebraically [46]

$$\begin{aligned} g_c(s) = & \frac{1}{(4\pi)^2} \left(\sigma \left[\log \left(\sigma \sqrt{1 + \frac{m_\rho^2}{q_{\rm max}^2}} + 1 \right) - \log \left(\sigma \sqrt{1 + \frac{m_\rho^2}{q_{\rm max}^2}} - 1 \right) \right] \right. \\ & \left. + 2 \log \left\{ \frac{m_\rho}{q_{\rm max}} \left(1 + \sqrt{1 + \frac{m_\rho^2}{q_{\rm max}^2}} \right) \right\} \right) \ . \end{aligned} \tag{24}$$

Typical values of the cutoff are around 1 GeV. The unitarity loop function $g(s)$ has a branch point at the $\rho\rho$ threshold ($s = 4m_\rho^2$) and a unitarity cut above it ($s > 4m_\rho^2$). The physical values of the T-matrix $T^{(JI)}(s)$, with $s > 4m_\rho^2$, are reached in the limit of vanishing positive imaginary part of s. Notice that the left-hand cut present in $V^{(JI)}(s)$ for $s < 3m_\rho^2$ does not overlap with the unitarity cut, so that $V^{(JI)}(s)$ is analytic in the complex s-plane around the physical s-axis for physical energies. In this way, the sign of the vanishing imaginary part of s for $V^{(JI)}(s)$ is of no relevance in the prescription stated above for reaching its value on the real axis with $s < 3m_\rho^2$ according to the Feynman rules.

We can also get a natural value for the subtraction constant a in Eq. (21) by matching $g(s)$ and $g_c(s)$ at threshold where $\sigma = 0$. For $\mu = m_\rho$, a usual choice, the final expression simplifies to

$$a = -2 \log \frac{q_{\rm max}}{m_\rho} \left(1 + \sqrt{1 + \frac{m_\rho^2}{q_{\rm max}^2}} \right) \ . \tag{25}$$

[3]It is the same result as calculating $g(s)$ in dimensional regularization, $d = 4 + 2\epsilon$, and replacing the $1/\epsilon$ divergence by a constant, cf. [46].

It is also worth noticing that Eq. (19) gives rise to a T-matrix $T^{(IJ)}(s)$ that is gauge invariance in the hidden local symmetry theory because this equation just stems from the partial-wave projection of a complete on-shell tree-level calculation within that theory, which certainly is gauge invariant.

3 Results

One of our aims is to check the stability of the results of Ref. [9] under relativistic corrections, particularly regarding the generation of the poles that could be associated with the $f_0(1370)$ and $f_2(1270)$ resonances as obtained in that paper. The main source of difference between our calculated $V^{(JI)}(s)$ and those in Ref. [9] arises from the different treatment of the ρ-meson propagator. The point is that the authors of Ref. [9] take the non-relativistic limit of this propagator so that from the expression $1/(t-m_\rho^2)$, cf. Eq. (8), or $1/(u-m_\rho^2)$, only $-1/m_\rho^2$ is kept. This is the reason that the tree-level amplitudes calculated in Ref. [9] do not have the branch point singularity at $s=3m_\rho^2$ nor the corresponding left-hand cut for $s<3m_\rho^2$. It turns out that for the isoscalar tensor case, the resonance $f_2(1270)$ is below this branch point, so that its influence cannot be neglected when considering the generation of this pole within this approach.

3.1 Uncoupled S-wave scattering

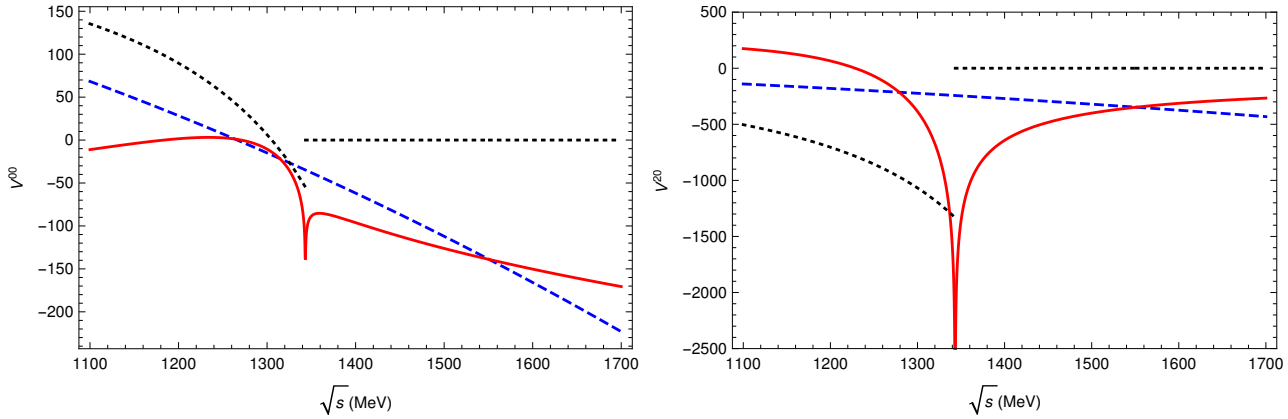
The issue on the relevance of this branch point singularity in the ρ-exchange amplitudes was not addressed in Ref. [9] and it is indeed very important. This is illustrated in Fig. 4 where we plot the potentials $V^{(JI)}(s)$ in S-wave ($\ell=0$) (only S-wave scattering is considered in Ref. [9]).[4] From top to bottom and left to right we show in the figure the potentials for the quantum numbers (J,I) equal to $(0,0)$, $(2,0)$, $(0,2)$, $(2,2)$ and $(1,1)$. The red solid and black dotted lines correspond to the real and imaginary parts of our full covariant calculation of the $V^{(JI)}(s)$, respectively, while the blue dashed ones are the results of Ref. [9]. The imaginary part in our results for $V^{(JI)}(s)$ appears below $s<3m_\rho^2$ due to the left-hand cut that arises from the t- and u-channel ρ-exchanges.

It can be seen that our results and those of Ref. [9] are typically close near threshold ($s=4m_\rho^2$) but for lower values of s they typically depart quickly due to the onset of the branch point singularity at $s=3m_\rho^2$. The strength of this singularity depends on the channel, being particularly noticeable in the $(J,I)=(2,0)$ channel, while for the $(0,0)$ channel it is comparatively weaker.

The strongest attractive potentials in the near threshold region occur for $(J,I)=(0,0)$ and $(2,0)$ and in every of these channels Ref. [9] found a bound-state pole that the authors associated with the $f_0(1370)$ and $f_2(1272)$ resonances, respectively. For the $(0,0)$ quantum numbers the pole position is relatively close to the $\rho\rho$ threshold, while for $(2,0)$ it is much further away. Two typical values of the cutoff $q_{\rm max}$ were used in Ref. [9], $q_{\rm max}=875$ MeV and 1000 MeV. We employ these values here, too, together with $q_{\rm max}=m_\rho$ (so that we consider three values of $q_{\rm max}$ separated by around 100 MeV), and study the pole positions for our $T^{(JI)}(s)$ amplitudes in S wave. We only find a bound state for the isoscalar scalar case, while for the tensor case no bound state is found. In Table 1 we give the values of the pole positions for our full calculation for $q_{\rm max}=m_\rho$ (first), 875 (second) and 1000 MeV (third row). For comparison we also give in round brackets the bound state masses obtained in Ref. [9], when appropriate. As indicated above, the strong differences for $V^{(20)}(s)$ between our full covariant calculation and the one in Ref. [9] in the extreme non-relativistic limit, cf. Fig. 4b, imply the final disappearance of the deep bound state for the isoscalar tensor case. The nominal three-momentum of a ρ around the mass of the $f_2(1270)$ has a modulus of about $0.6m_\rho\simeq 460$ MeV and for such high values of three-momentum relativistic corrections are of importance, as explicitly calculated here. On the contrary, the $(0,0)$ pole is located closer to the $\rho\rho$

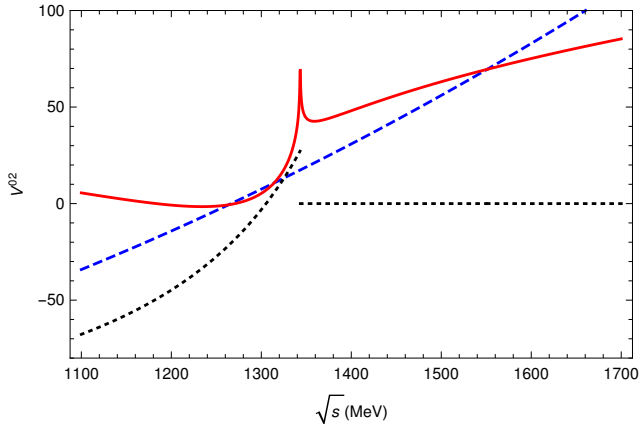
[4] Partial waves with $\ell\neq 0$ are considered in Sec. 3.2.

threshold and the results are more stable against relativistic corrections, though one still finds differences of around 20 MeV in the bound state mass.

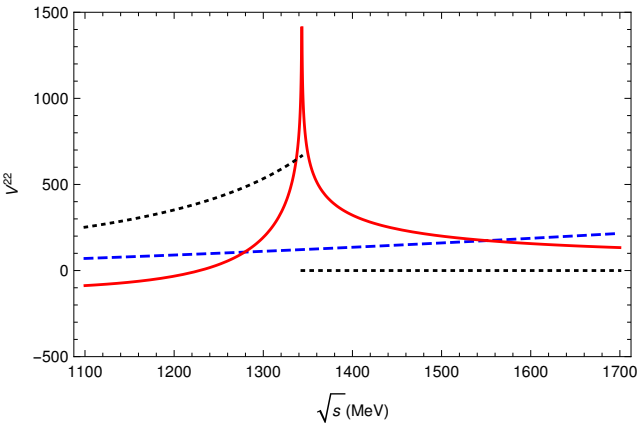


(a) $V^{(00)}(s)$

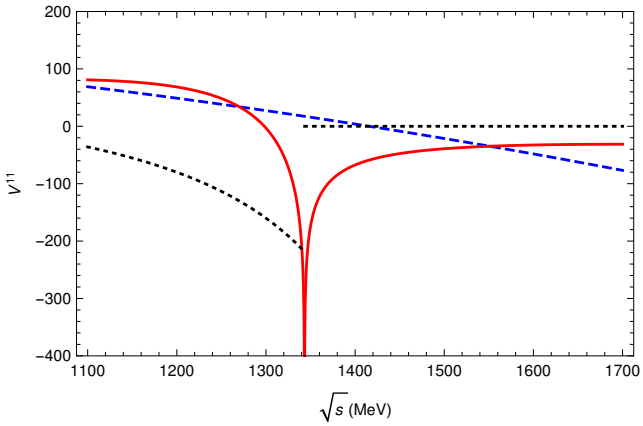
(b) $V^{(20)}(s)$



(c) $V^{(02)}(s)$



(d) $V^{(22)}(s)$



(e) $V^{(11)}(s)$

Figure 4: S-wave potentials $V^{(JI)}(s)$ (in MeV) for our calculation (real part: red solid line, imaginary part: black dotted line) and for the calculation of Ref. [9] (blue dashed lines).

$q_{\rm max}$ (MeV)	Pole Position (MeV) (Mass in Ref. [9])	$(\gamma_{00}^{(00)})^2$ (GeV^2)	$X_{00}^{(00)}$
775	1515.9	55	0.73
875	1494.8 (1512)	64	0.63
1000	1467.2 (1491)	68	0.52
775 (conv.)	1521.9		
875 (conv.)	1501.6		
1000 (conv.)	1475.6		

Table 1: Pole position for the partial wave $T^{(00)}(s)$ (2nd column), residue (3rd column) and compositeness (4th column) as a function of the three-momentum cutoff q_{max} (1st column). In the last three rows we take into account the finite width of the ρ in the evaluation of the $g(s)$ function, as indicated between parenthesis by (conv). For details, see the text.

In addition we also show in the third column of Table 1 the residue of $T^{(00)}(s)$ at the pole position s_P. For a generic partial wave $T^{(JI)}_{\ell S;\bar{\ell}\bar{S}}(s)$, its residue at a pole is denoted by $\gamma^{(JI)}_{\ell S}\gamma^{(JI)}_{\bar{\ell}\bar{S}}$ and is defined as

$$\gamma^{(JI)}_{\ell S}\gamma^{(JI)}_{\bar{\ell}\bar{S}} = -\lim_{s\to s_P}(s-s_P)T^{(JI)}_{\ell S;\bar{\ell}\bar{S}}(s)\ . \tag{26}$$

In terms of these couplings one can also calculate the compositeness $X^{(JI)}_{\ell S}$ associated with this bound state [47–49],

$$X^{(JI)}_{\ell S} = -\,{\gamma^{(JI)}_{\ell S;\ell S}}^{\,2}\,\frac{\partial g(s)}{\partial s}\Big|_{s_P}\ , \tag{27}$$

which in our case determines the $\rho\rho$ component in such bound state. Notice that the derivative of $g(s)$ from Eq. (21) (which is negative below threshold) does not depend on the subtraction constant, the dependence on the latter enters implicitly by the actual value of the pole position s_P. Of course, if one uses a three-momentum cutoff then $g_c(s)$ must be employed in the evaluation of $X^{(JI)}_{\ell S}$. The compositeness obtained for the pole positions in Table 1 is given in the fourth column of the same table. As expected the $\rho\rho$ component is dominant, with $X^{(00)}_{00} > 0.5$, and increases as the pole moves closer to threshold, so that it is 73% for $q_{\rm max} = m_\rho$ and $\sqrt{s_P} = 1516$ MeV.

We can also determine the pole positions when $g(s)$ is calculated with exact analytical properties, Eq. (21), and taking for a the values from Eq. (25) as a function of $q_{\rm max}$. The results are given Table 2, where we also give the residue at the pole position and the calculated compositeness, in the same order as in Table. 1. The results obtained are quite close to those in this table so that we refrain of further commenting on them. Nonetheless, we should stress again that we do not find any pole for the isoscalar tensor case.

We could try to enforce the generation of an isoscalar tensor pole by varying $q_{\rm max}$, when using $g_c(s)$, or by varying a, if Eq. (21) is used. In the former case a much lower value of $q_{\rm max}$ is required than the chiral expansion scale around 1 GeV ($q_{\rm max} \lesssim 400$ MeV), while for the latter a qualitatively similar situation arises when taking into account the relationship between a and $q_{\rm max}$ of Eq. (25). Even more serious are two facts that happen in relation with this isoscalar tensor pole. First one should stress that such pole appears associated to the evolution with $q_{\rm max}$ or a of a pole in the first Riemann sheet, which violates

a	Pole Position (MeV)	$(\gamma_{00}^{(00)})^2$ (GeV^2)	$X_{00}^{(00)}$
-1.697	1525.7	43	0.80
-1.938	1500.4	56	0.69
-2.144	1474.5	62	0.58
-1.697 (conv.)	1546.0		
-1.938 (conv.)	1517.7		
-2.144 (conv.)	1491.1		

Table 2: Pole positions for the partial wave $T^{(00)}(s)$ (2nd column), residue (3rd column) and compositeness (4th column) as a function of the subtraction constant a (1st column). In the last three rows we take into account the finite width of the ρ in the evaluation of the $g(s)$ function, this is indicated between parenthesis by (conv).

analyticity. This is shown in Fig. 5 where we exhibit the evolution of this pole as a function of $q_{\rm max}$. We start the series at a low value of $q_{\rm max} = 300$ MeV, where we have two poles on the real axis, and increase the cutoff in steps of $\delta q_{\rm max} = 50$ MeV. These two poles get closer and merge for $q_{\rm max} = 403.1$ MeV. For larger values of the cutoff the resulting pole moves deeper into the complex plane of the physical or first Riemann sheet. Second, we obtain that $X_{02}^{(20)}$ is larger than 1. For example, for $q_{\rm max} = 400$ MeV, there are two poles at 1422.4 and 1463.4 MeV with $X_{02}^{(20)} = 2.7$ and 3.8, in order, which of course makes no sense as compositeness factors have to be less or equal to one.

Next, we take into account the finite width of the ρ meson in the evaluation of the unitarity two-point loop function $g(s)$. As a result the peak in the modulus squared of the isoscalar scalar amplitude now acquires some width due to the width itself of the ρ meson. To take that into account this effect we convolute the $g(s)$ function with a Lorentzian mass squared distribution for each of the two ρ mesons in the intermediate state [9, 33]. The resulting unitarity loop function is denoted by $\mathfrak{g}(s)$ and is given by

$$\mathfrak{g}(s) = \frac{1}{N^2}\int_{(m_\rho-2\Gamma_\rho)^2}^{(m_\rho+2\Gamma_\rho)^2} dm_1^2 \frac{\Gamma m_1/\pi}{(m_1^2-m_\rho^2)^2+m_1^2\Gamma^2}\int_{(m_\rho-2\Gamma_\rho)^2}^{(m_\rho+2\Gamma_\rho)^2} dm_2^2 \frac{\Gamma m_2/\pi}{(m_2^2-m_\rho^2)^2+m_2^2\Gamma^2} g(s,m_1^2,m_2^2)\ . \quad (28)$$

The normalization factor N is

$$N = \int_{(m_\rho-2\Gamma_\rho)^2}^{(m_\rho+2\Gamma_\rho)^2} dm^2 \frac{\Gamma m/\pi}{(m^2-m_\rho^2)^2+m^2\Gamma^2}\ , \quad (29)$$

with $\Gamma(m)$ the width of the ρ meson with mass m. Due to the P-wave nature of this decay to $\pi\pi$, we take into account its strong cubic dependence on the decaying pion three-momentum and use the approximation

$$\Gamma(m) = \Gamma_\rho \left(\frac{m^2-4m_\pi^2}{m_\rho^2-4m_\pi^2}\right)^3 \theta(m-2m_\pi) \quad (30)$$

with m_π the pion mass and $\Gamma_\rho \cong 148$ MeV [5]. The function $g(s,m_1^2,m_2^2)$ is the two-point loop function with different masses, while in Eq. (21) we give its expression for the equal mass case. When evaluated

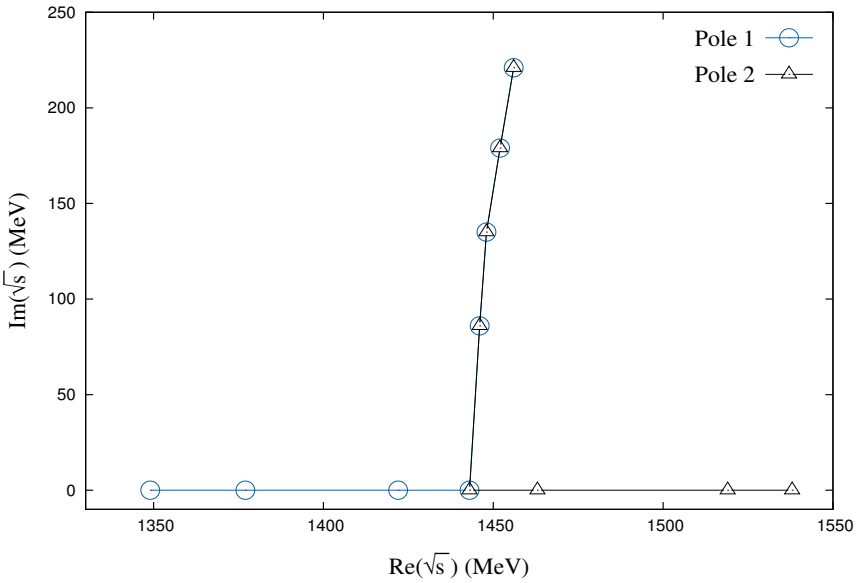


Figure 5: Evolution of the poles in the physical Riemann sheet for the isoscalar tensor channel as a function of $q_{\rm max}$. Two poles are present on the real axis for our starting value of $q_{\rm max} = 300$ MeV, and along the trajectory we increase $q_{\rm max}$ in steps of $\delta q_{\rm max} = 50$ MeV. The two poles merge at $q_{\rm max} = 403.1$ MeV and for larger values of the cutoff there is one pole that moves deeper into the complex plane.

in terms of a dispersion relation it reads,

$$\begin{aligned} g(s, m_1^2, m_2^2) =& \frac{1}{16\pi^2}\Bigg\{ a(\mu) + \log\frac{m_1^2}{\mu^2} + \frac{s - m_1^2 + m_2^2}{2s}\log\frac{m_2^2}{m_1^2} \\ &+ \frac{\lambda^{1/2}(s)}{2s}\Bigg[\log\left(\lambda^{1/2}(s) + s - m_2^2 + m_1^2\right) - \log\left(\lambda^{1/2}(s) - s + m_2^2 - m_1^2\right) \\ &+ \log\left(\lambda^{1/2}(s) + s + m_2^2 - m_1^2\right) - \log\left(\lambda^{1/2}(s) - s - m_2^2 + m_1^2\right)\Bigg]\Bigg\}\,, \end{aligned} \tag{31}$$

with $\lambda^{1/2}(s) = \sqrt{s^2 + m_1^4 + m_2^4 - 2sm_1^2 - 2sm_2^2 - 2m_1^2m_2^2}$. The algebraic expression of this function when calculated with a three-momentum cutoff for different masses can be found in Ref. [46], to which we refer the interested reader.

When using the convoluted $g(s)$ function we find similar masses for the peak of $|T^{(00)}|^2$ in the $(0,0)$ channel compared to the case without convolution. The resulting peak positions are given in the last three rows of Tables 1 and 2. The effects of the non-zero ρ width are clearly seen in Fig. 6, where we plot $|T^{(00)}(s)|^2$ for the different values of $q_{\rm max}$ shown in Table 1. The shape of the peaks follows quite closely a Breit-Wigner form, though it is slightly wider to the right side of the peak. We find that the width decreases with the increasing value of $q_{\rm max}$, being around 45, 65 and 95 MeV for $q_{\rm max} = 1000$, 875 and 775 MeV, respectively, of similar size as those found in Ref. [9]. When using a subtraction constant instead of $q_{\rm max}$, relating them through Eq. (25), the picture is quite similar. The peak positions are given in the last three columns of Table 2 while the widths obtained are around 105, 70 and 50 MeV for $a = -1.70$, -1.94 and -2.14, in order. These widths are significantly smaller than the PDG values assigned to the $f_0(1370)$ resonance of 200-500 MeV [5].

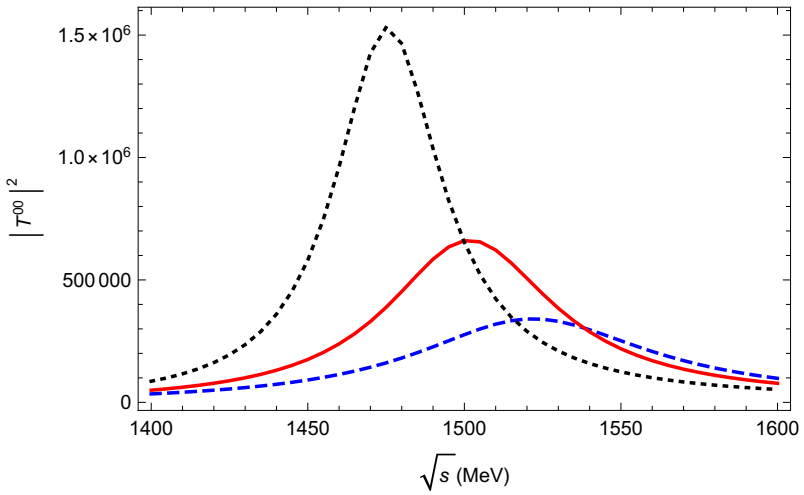


Figure 6: The amplitude squared $|T^{00}|^2$ when using the convoluted $g(s)$ function with a cutoff $q_{\rm max}$. The blue dashed line corresponds to $q_{\rm max} = 775$ MeV, the red solid one to 875 MeV and the black dotted one to 1000 MeV.

Due to the coupling of the $\rho\rho$ and $\pi\pi$, this pole could develop a larger width. This is approximated in Ref. [9] by considering the imaginary part of the $\pi\pi$ box diagram, with a $\rho \to \pi\pi$ vertex at each of the vertices of the box. These vertices are also worked out from the non-linear chiral Lagrangian with hidden gauge symmetry [27, 28]. We refer to Ref. [9] for details on the calculation of this contribution. According to this reference one has to add to $V^{(00)}_{00;00}$ and to $V^{(20)}_{02;02}$ the contribution $V^{(JI)}_{2\pi}$, given by

$$\begin{aligned} V^{(00)}_{2\pi} =& 20i\,{\rm Im}\widetilde{V}_{\pi\pi}\ , \\ V^{(20)}_{2\pi} =& 8i\,{\rm Im}\widetilde{V}_{\pi\pi}\ . \end{aligned} \tag{32}$$

In the calculation of the function $\widetilde{V}_{\pi\pi}$, Ref. [9] introduces a monopole form factor $F(q)$ for each of the four $\rho \to \pi\pi$ vertices in the pion box calculation,

$$F(q) = \frac{\Lambda^2 - m_\pi^2}{\Lambda^2 - (k-q)^2} \tag{33}$$

with $k^0 = \sqrt{s}/2$, $\mathbf{k} = 0$, $q^0 = \sqrt{s}/2$ and $\mathbf{q}$ the integration variables. This introduces a sizeable dependence of the results on the value of Λ. Nonetheless, in order to compare with Ref. [9] we follow the very same scheme of calculation and take the same values for Λ, that is, 1200, 1300 and 1400 MeV.[5]

The inclusion of the $\pi\pi$ box diagram, on top of the convolution with the ρ mass squared distribution for calculating the $g(s)$ function, does not alter the previous conclusion on the absence of a pole in the isoscalar tensor channel. However, the isoscalar scalar pole develops a larger width around 200-300 MeV, that increases with Λ, as can be inferred from Fig. 7, where we plot $|T^{(00)}(s)|^2$. On the other hand, the position of the peak barely changes compared to the one given in the last two rows of Table 1.Tentatively this pole could be associated to the $f_0(1370)$ resonance, which according to Refs. [50, 51] decays mostly

[5]Another more complete scheme is two work explicitly with coupled-channel scattering as done in Ref. [50], where $\rho\rho$ and $\pi\pi$ channels, among many others, were explicitly included. In this way resonances develop decay widths in a full nonperturbative fashion because of the coupling between channels.

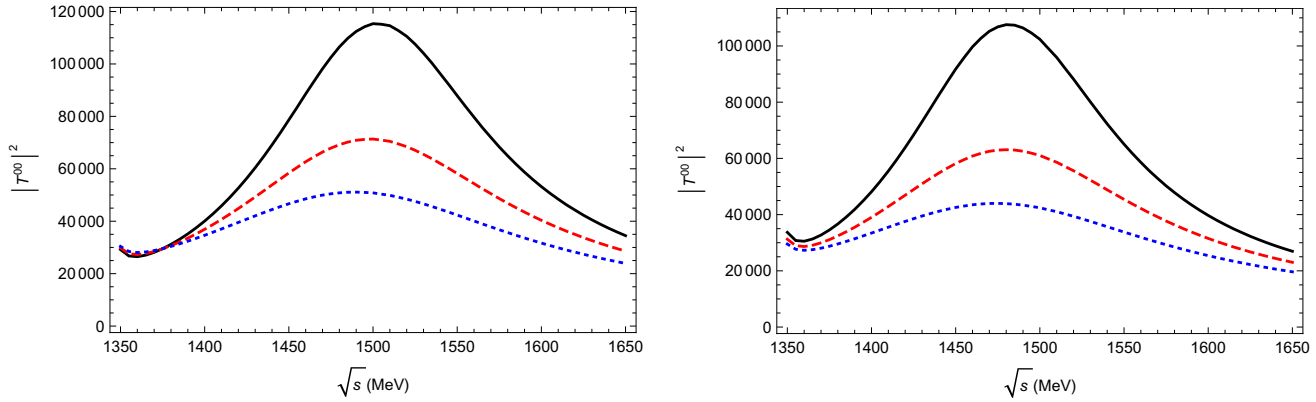


Figure 7: $|T^{(00)}(s)|^2$ with the $\pi\pi$ box diagram contribution included for different values of Λ in $F(q)$, cf. Eq. (33). Specifically, $\Lambda = 1200$ (black solid line), 1300 (red dashed line) and 1400 MeV (blue dotted line), for $q_{\rm max} = 875$ (left panel) and $q_{\rm max} = 1000$ MeV (right panel).

(J, I)	(ℓ, S) channels
$(0, 0)$	$(0, 0)$, $(2, 2)$
$(2, 0)$	$(0, 2)$, $(2, 0)$, $(2, 2)$

Table 3: Coupled-channels with different orbital angular momentum.

to $\pi\pi$ with a width around 200 MeV. In the PDG [5] the total width of the $f_0(1370)$ is given with a large uncertainty, within the range 200-500 MeV and the $\pi\pi$ decay mode is qualified as dominant. The nearby $f_0(1500)$ resonance has a much smaller width, around 100 MeV, and its coupling and decay to $\pi\pi$ is suppressed. These properties of the $f_0(1500)$ are discussed in detail in Ref. [50].

3.2 Coupled-channel scattering

We now consider the impact on our results when allowing for the coupling between channels with different orbital angular momenta, an issue not considered in Ref. [9]. In Table 3 we show the different channels that couple for given JI quantum numbers and pay special attention to the $(J, I) = (0, 0)$ and $(2, 0)$ channels. Apart from the conservation of J and I, one also has to impose invariance under parity, which avoids the mixing between odd and even ℓ's.

When including coupled channel effects, one finds two poles in the channels with $(J, I) = (0, 0)$, that are reported in Table 4 for various values of $q_{\rm max}$ (shown in the first column). We give from left to right the pole mass (second column), the residues (third and fourth ones) and compositeness coefficients (fifth and sixth ones) of the different channels, $(\ell, S) = (0, 0)$ and $(2, 2)$, respectively. One of the poles is heavier and closer to the $\rho\rho$ threshold with similar properties as the pole in the uncoupled case, compare with Table 1, particularly for $q_{\rm max} = 775$ MeV. Nonetheless, as $q_{\rm max}$ increases the difference of the properties of this pole between the coupled and uncoupled cases is more pronounced. In particular let us remark that now $X_{00}^{(00)}$ is always $\gtrsim 0.7$ and for $q_{\rm max} = 1$ GeV the residue to the channel $(\ell, S) = (0, 0)$ is much larger than in the uncoupled case. Additionally, we find now a lighter pole which lays above the branch point singularity at $\sqrt{3}\, m_\rho \simeq 1343$ MeV. For lower values of the cutoff $q_{\rm max}$ this pole couples more strongly

$q_{\rm max}$ (MeV)	Mass (MeV)	$(\gamma_{00}^{(00)})^2$ (GeV^2)	$(\gamma_{22}^{(00)})^2$ (GeV^2)	$X_{00}^{(00)}$	$X_{22}^{(00)}$
775	1515.3	57.2	0.2	0.75	0.00
	1386.6	-7.6	-20.2	< 0	< 0
875	1492.4	72.1	1.0	0.69	0.01
	1396.8	-13.5	-19.4	< 0	< 0
1000	1455.3	116.2	8.3	0.80	0.06
	1415.7	-53.1	-25.1	< 0	< 0

Table 4: Bound state poles in the partial wave amplitudes of quantum numbers $(J, I) = (0, 0)$ with varying cutoff $q_{\rm max}$, which is indicated in the first column. The masses (2nd column), the residues to $(\ell, S) = (0, 0)$ and $(2, 2)$ (3rd and 4th columns) and the compositeness coefficients $X_{00}^{00)}$ and $X_{22}^{00)}$ (6th and 7th columns) are also given. For the lighter poles the compositeness coefficients are small and negative, so that they cannot be interpreted as physical states contrary to common wisdom [47–49].

to the $(\ell, S) = (2, 2)$ channel, but as the cutoff increases its residue for the channel $(\ell, S) = (0, 0)$ also increases in absolute value and it is the largest for $q_{\rm max} = 1$ GeV. It is then clear that both channels $(\ell, S) = (0, 0)$ and $(2, 2)$ are relevant for the origin of this pole. Note that the residues for this lighter pole are negative, which is at odds with the standard interpretation of the residue $(\gamma_{\ell S}^{(00)})^2$ of a bound state as the coupling squared. This implies that the compositeness coefficients $X_{\ell S}^{(00)}$ are all negative, which is at odds with a probabilistic interpretation as suggested in Refs. [47–49] for bound states. The moduli of the $|X_{\ell S}^{(00)}|$ are all small because this lighter pole lays quite far from the $\rho\rho$ threshold. The fact that its mass is not far from the strong branch point singularity at $\sqrt{3}\, m_\rho$ makes that this pole is very much affected by the left-hand cut discontinuity. In this respect, it might well be that the presence of this pole with anomalous properties is just an artefact of the unitarization formula of Eq. (19), that treats the left-hand cut discontinuity of the potential perturbatively. One can answer this question by solving exactly the N/D method [52, 53], so that the left-hand cut discontinuity of the potential is properly treated and the resulting amplitude has the right analytical properties. Let us recall that Eq. (19) is an approximate algebraic solution of the N/D method by treating perturbatively the left-hand cut discontinuities of the coupled partial waves [29, 36, 38]. For the uncoupled scattering such effects are further studied in detail in the next section.

$q_{\rm max}$ (MeV)	Mass (MeV)	$(\gamma_{02}^{(20)})^2$ (GeV^2)	$(\gamma_{20}^{(20)})^2$ (GeV^2)	$(\gamma_{22}^{(20)})^2$ (GeV^2)
775	1355.1	-0.8	-0.0	-8.6
875	1358.2	-0.7	-0.0	-8.3
1000	1361.8	-0.6	-0.0	-7.9

Table 5: Bound state poles in the partial wave amplitudes of quantum numbers $(J, I) = (2, 0)$ with different cutoffs $q_{\rm max}$, indicated in the first column. The masses (2nd column) and the residues to $(\ell, S) = (0, 2)$, $(2, 0)$ and $(2, 2)$ (3rd, 4th and 5th columns) are shown. Here, "-0.0" denotes a small but negative number.

For the $(J, I) = (2, 0)$ partial waves we have three coupled channels, $(\ell, S) = (0, 2)$, $(2, 0)$ and $(2, 2)$ and, contrary to the uncoupled case, we now find a pole that lays above the branch point singularity. We give its mass and residues for different $q_{\rm max}$ in Table 5, with the same notation as in Table 4. Notice that

these pole properties are very stable under the variation of $q_{\rm max}$. This pole couples by far much more strongly to the channel with $(\ell, S) = (2, 2)$ than to any other channel. This indicates that it is mainly due to the dynamics associated with the $(\ell, S) = (2, 2)$ channel. But the same comments are in order here as given above for the lighter isoscalar scalar pole, because its residues shown in Table 5 are negative and so are the corresponding compositeness coefficients. Hence, the lighter pole for $(J, I) = (0, 0)$ and the one found for $(2, 2)$ cannot be considered as robust results of our analysis. This has to be contrasted to the case of the heavier isoscalar scalar pole that is stable under relativistic corrections, coupled-channel effects and has quite standard properties regarding its couplings and compositeness coefficients.

4 First iterated solution of the N/D method

In this section for definiteness we only consider uncoupled scattering. We have in mind the $(J, I) = (0, 0)$ and $(J, I) = (2, 0)$ quantum numbers to which special attention has been paid in the literature concerning the generation of poles that could be associated with the $f_0(1370)$ and $f_2(1270)$ resonances, as discussed above. Further applications of the improved unitarization formalism presented in this section are left for future work.

According to the N/D method [54] a partial-wave amplitude can be written as

$$T = \frac{N(s)}{D(s)} \, , \tag{34}$$

where the function $D(s)$ has only the unitarity or right-hand cut (RHC) while $N(s)$ only has the left-hand cut (LHC). The secular equation for obtaining resonances and bound states corresponds to look for the zeros of $D(s)$,

$$D(s_i) = 0 \, . \tag{35}$$

Below threshold along the real s axis this equation is purely real because $D(s)$ has a non-vanishing imaginary part only for $s > s_{\rm th}$.

However, with our unitarization procedure from leading-order unitary chiral perturbation theory (UChPT) we have obtained the approximation

$$T^{(JI)}(s) = \frac{V^{(JI)}(s)}{1 - V^{(JI)}(s) g_c(s)} \, , \tag{36}$$

and the resulting equation to look for the bound states is

$$D_U(s) = 1 - V(s) g_c(s) = 0 \, . \tag{37}$$

Notice that Eq. (36), contrary to the general Eq. (35), has an imaginary part below the branch-point singularity at $s = 3m^2$.

We can go beyond this undesired situation by considering the first-iterated solution to the N/D method. This is indeed similar to Eq. (36) but improving upon it because it allows us to go beyond the on-shell factorization employed in this equation. In the first-iterated N/D solution one identifies the numerator function $N(s)$ to the tree-level calculation $V^{(JI)}(s)$ and employs the exact dispersive expression

for $D(s)$. Namely, it reads[6]

$$
\begin{aligned}
N(s) &= V^{(JI)}(s) \ , \\
D(s) &= \gamma_0 + \gamma_1 (s - s_{th}) + \frac{1}{2}\gamma_2 (s - s_{s_{\rm th}})^2 + \frac{(s - s_{\rm th})s^2}{\pi} \int_{s_{\rm th}}^{\infty} ds' \frac{\rho(s') V^{(JI)}(s')}{(s' - s_{\rm th})(s' - s)(s')^2} \ , \\
T_{ND}(s) &= \frac{N(s)}{D(s)} \ ,
\end{aligned}
\tag{38}
$$

with the phase space factor $\rho(s)$ given by $\rho(s) = \sigma(s)/16\pi$. We have taken three subtractions in the dispersion relation for $D(s)$ because $V^{(JI)}(s)$ diverges as s^2 for $s \to \infty$.

From our present study we have concluded that $T^{(JI)}(s)$ is stable in the threshold region under relativistic corrections as well as under the addition of coupled channels. Because of the stability of the results in this region under relativistic corrections and by visual inspection of the potentials in Fig. 4 one concludes that the near-threshold region is quite safe of the problem related to the branch-point singularity of the LHC associated with one-ρ crossed-channel exchanges. We then determine the subtractions constants, γ_0, γ_1 and γ_2 in $D(s)$ by matching $T_{ND}(s)$, Eq. (38), and $T^{(JI)}(s)$, Eq. (36), around threshold ($s_{\rm th}$). At the practical level it is more convenient to match $1/T(s)$, so that in the threshold region up to $\mathcal{O}(s^3)$ one has:

$$
\begin{aligned}
\gamma_0 + \gamma_1 (s - s_{th}) + \frac{1}{2}\gamma_2 (s - s_{s_{\rm th}})^2 &= 1 - V(s) g_c(s) - \frac{(s - s_{\rm th})s^2}{\pi} \int_{s_{\rm th}}^{\infty} ds' \frac{\rho(s') V(s')}{(s' - s_{\rm th})(s' - s)(s')^2} \\
&\equiv \omega(s) \ .
\end{aligned}
\tag{39}
$$

In this way,

$$
\begin{aligned}
\gamma_0 &= 1 - V(s_{\rm th}) g_c(s_{\rm th}) \ , \\
\gamma_1 &= \omega'(s_{\rm th}) \ , \\
\gamma_2 &= \omega''(s_{\rm th}) \ .
\end{aligned}
\tag{40}
$$

The dependence of our present results on the cutoff used in $T^{(JI)}(s)$ stems from the matching conditions of Eq. (40). However, let us stress that the analytical properties of $D(s)$ and $N(s)$ are correct, they have the RHC and LHC with the appropriate extent and branch point singularities, respectively, and the resulting amplitude is unitarized.

4.1 Results $J = 0$, $I = 0$

We plot $D(s)$ for $(J, I) = (0, 0)$ in Fig. 8 for $q_{\rm max} = 0.7$, 1 and 1.3 GeV by the red solid, green dashed and blue dash-dotted lines, in order. The crossing with the zero line (dotted one) indicates the mass of the bound state. This mass decreases with increasing $q_{\rm max}$, being around 1.4 GeV for the largest cutoff and very close to threshold for the smallest. In Fig. 9 we compare the real (left) and imaginary parts (right panel) of $D(s)$ and $D_U(s) = 1 - V(s) g_c(s)$ for a cutoff of 1 GeV. We do not show more values of the cutoff because the same behavior results. The function $D(s)$ and $D_U(s)$ match up to around the branch-point singularity at $\sqrt{s} = 3m_\rho^2$. Below it $D_U(s)$ becomes imaginary, cf. Eq. (37), while $D(s)$ remains real and has this right property by construction, cf. Eq. (38). Above threshold the imaginary parts of both functions coincide as demanded by unitarity. We see that for these quantum numbers our

[6] A comprehensive introduction to the N/D method is given in Refs. [29, 53, 55, 56].

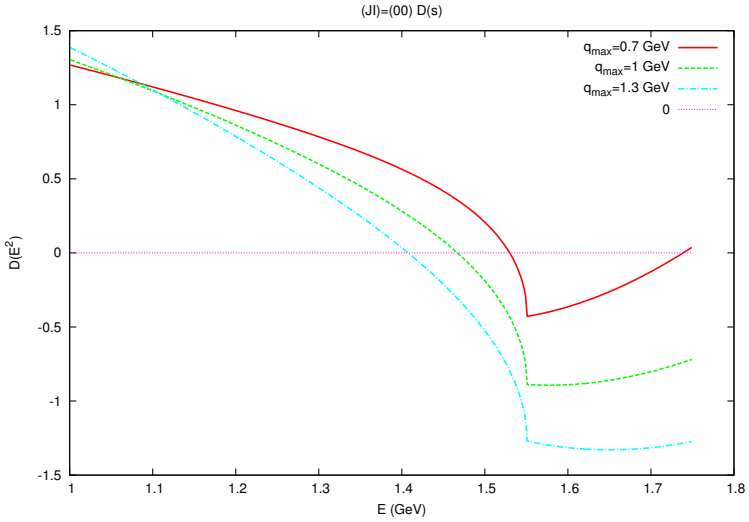


Figure 8: $D(s)$ function, Eq. (38), for $(J, I) = (0, 0)$. Above threshold only the real part is shown.

new improved unitarization formalism and the one used to derive Eq. (19) agree very well. The bound-state mass remains the same as given in Table 1 because the functions $D(s)$ and $D_U(s)$ match perfectly well in the region where these poles occur, as it is clear from Fig. 9. This should be expected because for $(J, I) = (0, 0)$ the branch point singularity was much weaker than for other cases, e.g. $(J, I) = (2, 0)$, as discussed above.

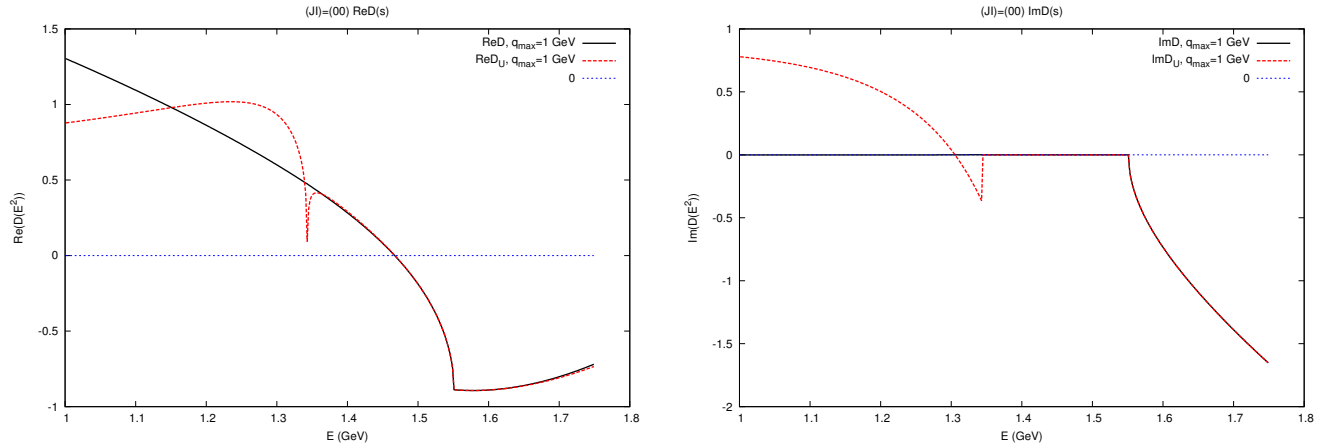


Figure 9: $(J, I) = (0, 0)$. Real (left) and imaginary (right panel) parts of $D(s)$ compared also with $D_U(s) = 1 - V^{(00)}(s)g_c(s)$ from leading-order UChPT.

4.2 Results $J = 2$, $I = 0$

We plot $D(s)$ for $(J, I) = (2, 0)$ in Fig. 10 for $q_{\rm max} = 0.7$, 1 and 1.3 GeV by the red solid, green dashed and blue dash-dotted lines, respectively. One can see that in this region the function $D(s)$ is large and

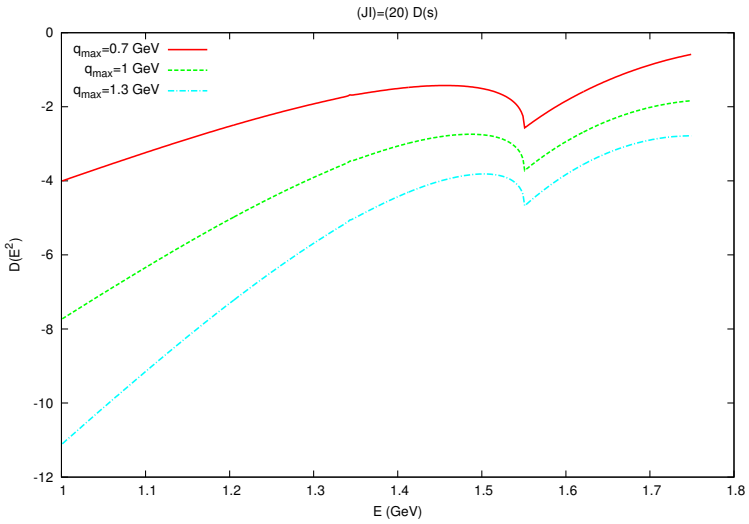


Figure 10: $D(s)$ function, Eq. (38), for $(J, I) = (2, 0)$. Above threshold only the real part is shown.

negative so that there is by far no pole in the $f_2(1270)$ region. In order to show the curves more clearly we use only $q_{\rm max} = 1$ GeV in Fig. 11, for other values of $q_{\rm max}$ the behavior is the same. In the left panel we compare the real parts of $T_{ND}(s)$ (black solid) and $T^{(20)}(s)$ (red dashed) while in the right panel we proceed similarly for the real parts of $D(s)$ and $D_U(s) = 1 - V^{(20)}(s)g_c(s)$, with the same type of lines in order. All the functions match near the threshold region and above it, but they strongly depart once we approach the LHC branch-point singularity at $s = 3m_\rho^2$ and beyond (for smaller values of s). Notice that $D(s)$, which has not such branch-point singularity, follows then the smooth decreasing trend already originated for $3m^2 < s < 4m^2$. For $(J, I) = (0, 0)$ the corresponding smooth trend is that of a decreasing function, cf. Fig. 8. The branch-point singularity is clearly seen in $T^{(20)}(s)$ because it is proportional to $V^{(20)}(s)$.

In summary, the conclusions obtained in Sec. 3.1 regarding the generation of the pole that could be identified with the $f_0(1370)$ and the absence of that associated with the $f_2(1270)$ as claimed in Ref. [9] fully hold. As a matter of fact, they get reinforced after considering the more elaborated unitarization process that is obtained here by taking the first-iterated N/D solution.

5 Summary and conclusions

In this paper, we have revisited the issue of resonance generation in unitarized $\rho\rho$ scattering using a chiral covariant formalism. The main results of our study can be summarized as follows:

i) We have developed a partial-wave projection formalism that is applicable to the covariant treatment of $\rho\rho$ scattering. In particular, we point out that accounting for the full ρ-meson propagator leads to a branch point in the partial wave projected amplitudes at $s = 3m_\rho^2 \simeq 1.8\,\text{GeV}^2$, about 208 MeV below the 2ρ threshold. This branch point does not appear in the extreme non-relativistic treatment of the propagator.

ii) Evaluating the T-matrix using the standard form, see Eq. (19) that treats the left-cut perturbatively, we find a pole in the scalar isoscalar channel close to the $\rho\rho$ threshold that can be associated with the

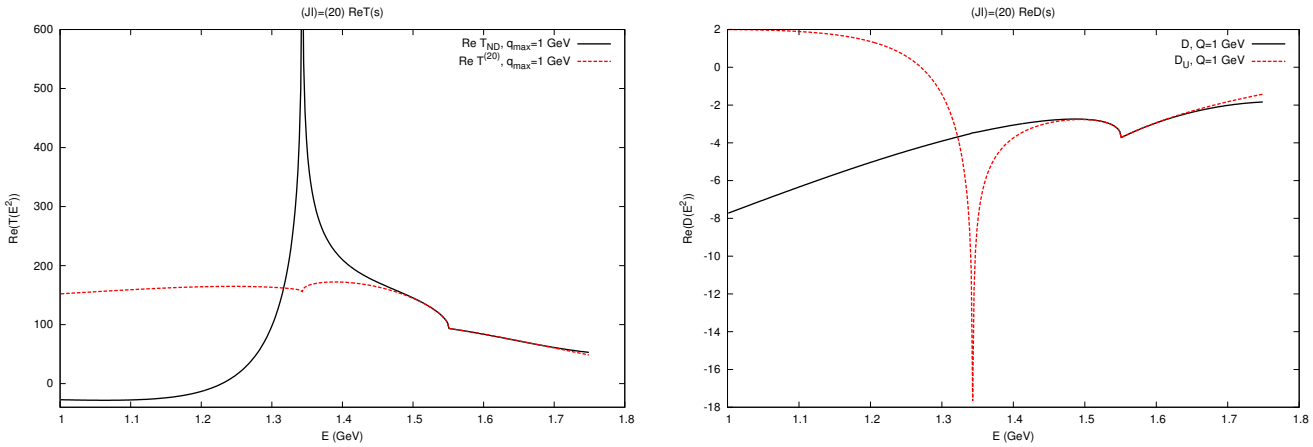


Figure 11: $(J, I) = (2, 0)$. Left panel: real part of $T_{ND}(s)$ (black solid) compared with that of $T^{(20)}(s)$ (red dashed). Right panel: comparison between the real parts of $D(s)$ (black solid) and $D_U(s) = 1 - V^{(20)}(s)g_c(s)$ (red dashed).

$f_0(1370)$ resonance, in agreement with the findings of Ref. [9], though there are minor quantitative differences.

iii) In contrast to Ref. [9], we do not find a tensor state below the scalar one. This can be traced back to the influence of the aforementioned branch point. We therefore conclude that the state that is identified in Ref. [9] with the $f_2(1270)$ is an artifact of the non-relativistic approximation and its generation does not hold from the arguments given in that reference.

iv) We have also worked out the effects of the coupling between channels with different orbital angular momenta, which lead to additional states. These, however, have negative composite coefficients and are thus not amenable to a simple bound state interpretation. As these states are close to the branch point at $s = 3m_\rho^2$, the perturbative treatment of the left-hand cut, as employed here, is certainly not sufficient to decide about their relevance.

v) We have improved the treatment of the left-hand cut by employing the first-iterated N/D method, in particular this method avoids the factorization approach of leading order UChPT. We worked the solutions that follow for uncoupled scattering in the $(J, I) = (0, 0)$ and $(2, 0)$ channels. The outcome fully agrees with the conclusions already obtained from UChPT and, notably, the absence of a pole that could be associated with the $f_2(1270)$ is firmly reinforced.

A lesson from points iii) and v) is clear. A strongly attractive interaction in a given channel is a necessary but by far not sufficient condition to generate a multi-hadron bound state. This argument, as used in Ref. [9], is in general terms too naive because it does not take into account the possible raise of a singularity in the true potential between the range of validity of the approximation used and the predicted bound-state mass from the latter. It could be rephrased as trying to deduce the values of the function $1/(1 + x)$ for $x < -1$ by knowing its values for x around 0.

We conclude that the approach presented here should be used to investigate the possible generation of meson resonances from the interaction of vector mesons. In the next steps, we will investigate how the

relativistic effects affect the conclusions of the SU(3) calculation of Ref. [10] and will further sharpen the framework along the lines mentioned, in particular by solving exactly the N/D equations [53].

Acknowledgements

We thank Maxim Mai for useful discussions and for his contribution during the early stages of this investigation. We would also like to thank E. Oset for some criticism which led us to add some additional material to the manuscript. This work is supported in part by the DFG (SFB/TR 110, "Symmetries and the Emergence of Structure in QCD"). JAO would like to acknowledge partial financial support from the MINECO (Spain) and ERDF (European Commission) grant FPA2013-40483-P and by the Spanish Excellence Network on Hadronic Physics FIS2014-57026-REDT. The work of UGM was supported in part by The Chinese Academy of Sciences (CAS) President's International Fellowship Initiative (PIFI) grant no. 2015VMA076.

A Partial-wave projection formalism

In this appendix we detail the projection formalism used in this work to calculate the different $\rho\rho$ partial waves. First, we give the expression for the polarization vectors for a massive spin-one particle with a three-momentum $\mathbf{p}$ and third component of spin σ in the z axis of its rest frame, that we denote by $\varepsilon(\mathbf{p},\sigma)$. In the rest frame they are given by

$$\varepsilon(\mathbf{0},\sigma) = \begin{pmatrix} 0 \\ \boldsymbol{\varepsilon}_\sigma \end{pmatrix} , \tag{A.1}$$

with

$$\boldsymbol{\varepsilon}_0 = \begin{pmatrix} 0 \\ 0 \\ 1 \end{pmatrix} , \; \boldsymbol{\varepsilon}_{\pm 1} = \frac{\mp 1}{\sqrt{2}} \begin{pmatrix} 1 \\ \pm i \\ 0 \end{pmatrix} . \tag{A.2}$$

Next, we take a Lorentz transformation $U(\mathbf{p})$ along the vector $\mathbf{p}$ that takes the particle four-momentum at rest to its final value,

$$U(\mathbf{p}) \begin{pmatrix} m \\ \mathbf{0} \end{pmatrix} = \begin{pmatrix} E_p \\ \mathbf{p} \end{pmatrix} , \tag{A.3}$$

with $E_p = \sqrt{m^2 + \mathbf{p}^2}$. We also introduce the rotation $R(\hat{\mathbf{p}})$ that takes $\hat{\mathbf{z}}$ to $\hat{\mathbf{p}}$,

$$R(\hat{\mathbf{p}})\hat{\mathbf{z}} = \hat{\mathbf{p}} . \tag{A.4}$$

In terms of the polar (θ) and azimuthal (ϕ) angles of $\hat{\mathbf{p}}$ this rotation is defined as

$$R(\hat{\mathbf{p}}) = R_z(\phi) R_y(\theta) , \tag{A.5}$$

with the subscripts z and y indicating the axis of rotation. For latter convenience we write the Lorentz transformation $U(\mathbf{p})$ as

$$U(\mathbf{p}) = R(\hat{\mathbf{p}}) B_z(|\mathbf{p}|) R(\hat{\mathbf{p}})^{-1} , \tag{A.6}$$

where $B_z(|\mathbf{p}|)$ is a boost along the $\hat{\mathbf{z}}$ axis with velocity $v=-\beta$ and $\beta=|\mathbf{p}|/E_p$. Namely,

$$B_z(|\mathbf{p}|)=\begin{pmatrix}\gamma & 0 & 0 & \gamma\beta\\ 0 & 0 & 0 & 0\\ 0 & 0 & 0 & 0\\ \gamma\beta & 0 & 0 & \gamma\end{pmatrix} \tag{A.7}$$

and

$$\gamma=\frac{1}{\sqrt{1-\beta^2}}\ . \tag{A.8}$$

Notice that one could also include any arbitrary rotation around the $\hat{\mathbf{z}}$ axis to the right end of Eq. (A.5). Of course, this does not have any affect on either Eqs. (A.4) and (A.6) (for the latter one let us note that $B_z(|\mathbf{p}|)$ commutes with a rotation around the $\hat{\mathbf{z}}$ axis).

The action of $U(\mathbf{p})$ on $\epsilon(\mathbf{0},\sigma_i)$ gives us the polarization vectors with definite three-momentum $\mathbf{p}$, whose expressions are

$$\varepsilon(\mathbf{p},0)=\begin{pmatrix}\gamma\beta\cos\theta\\ \frac{1}{2}(\gamma-1)\sin 2\theta\cos\phi\\ \frac{1}{2}(\gamma-1)\sin 2\theta\sin\phi\\ \frac{1}{2}\left(1+\gamma+(\gamma-1)\cos 2\theta\right)\end{pmatrix}\ ,\ \varepsilon(\mathbf{p},\pm1)=\mp\frac{1}{\sqrt{2}}\begin{pmatrix}\gamma\beta e^{\pm i\phi}\sin\theta\\ 1+(\gamma-1)e^{\pm i\phi}\sin^2\theta\cos\phi\\ \pm i+(\gamma-1)e^{\pm i\phi}\sin^2\theta\sin\phi\\ \frac{1}{2}(\gamma-1)e^{\pm i\phi}\sin 2\theta\end{pmatrix}\ . \tag{A.9}$$

The previous equation can be written in more compact form as

$$\varepsilon(\mathbf{p},\sigma)=\begin{pmatrix}\gamma\beta\hat{\mathbf{p}}\cdot\boldsymbol{\varepsilon}_\sigma\\ \boldsymbol{\varepsilon}_\sigma+\hat{\mathbf{p}}\,(\gamma-1)\hat{\mathbf{p}}\cdot\boldsymbol{\varepsilon}_\sigma\end{pmatrix}\ . \tag{A.10}$$

In terms of the polarization vectors in Eq. (A.10) we can write the vector field for the neutral ρ^0 particle, $\rho^0_\mu(x)$, as

$$\rho^0_\mu(x)=\sum_\sigma\int\frac{d^3p}{(2\pi)^3 2E_p}\left\{\varepsilon(\mathbf{p},\sigma)_\mu e^{-ip\,x}a(\mathbf{p},\sigma)+\varepsilon(\mathbf{p},\sigma)^*_\mu e^{ip\,x}a(\mathbf{p},\sigma)^\dagger\right\}\ , \tag{A.11}$$

with the corresponding similar expressions for the $\rho^\pm(x)$ fields. Here $a(\mathbf{p},\sigma)$ and $a(\mathbf{p},\sigma)^\dagger$ refer to the annihilation and creation operators, with the canonical commutation relation

$$[a(\mathbf{p}',\sigma'),a(\mathbf{p},\sigma)^\dagger]=\delta_{\sigma\sigma'}(2\pi)^3 2E_p\delta(\mathbf{p}-\mathbf{p}')\ . \tag{A.12}$$

In order to check the time-reversal and parity-invariance properties of the vector-vector scattering amplitudes worked out from the chiral Lagrangians in Eq. (1) we notice that the polarization vectors in Eq. (A.9) satisfy the following transformation properties:

$$\begin{aligned}\varepsilon(-\mathbf{p},\sigma)^*=&(-1)^\sigma(-\varepsilon(\mathbf{p},\sigma)_0,\boldsymbol{\varepsilon}(\mathbf{p},\sigma))\ ,\\ \varepsilon(-\mathbf{p},\sigma)=&(-\varepsilon(\mathbf{p},\sigma)_0,\boldsymbol{\varepsilon}(\mathbf{p},\sigma))\ .\end{aligned} \tag{A.13}$$

A one-particle state $|\mathbf{p},\sigma\rangle$ is obtained by the action of the creation operators on the vacuum state,

$$|\mathbf{p},\sigma\rangle=a(\mathbf{p},\sigma)^\dagger|\mathbf{0},\sigma\rangle\ . \tag{A.14}$$

From Eq. (A.12) it follows the following normalization for such states

$$\langle \mathbf{p}', \sigma' | \mathbf{p}, \sigma \rangle = \delta_{\sigma'\sigma} (2\pi)^3 2E_p \delta(\mathbf{p}' - \mathbf{p}) \ . \tag{A.15}$$

Next, we consider a two-body state characterized by the CM three-momentum $\mathbf{p}$ and the third components of spin σ_1 and σ_2 in their respective rest frames. This state is denoted by $|\mathbf{p}, \sigma_1\sigma_2\rangle$. Associated to this, we can define the two-body state with orbital angular momentum ℓ with its third component of orbital angular momentum m, denoted by $|\ell m, \sigma_1\sigma_2\rangle$ as

$$|\ell m, \sigma_1\sigma_2\rangle = \frac{1}{\sqrt{4\pi}} \int d\hat{\mathbf{p}}\, Y_\ell^m(\hat{\mathbf{p}}) |\mathbf{p}, \sigma_1\sigma_2\rangle \ . \tag{A.16}$$

Let us show first that this definition is meaningful because the state $|\ell m, \sigma_1\sigma_2\rangle$ transforms under the rotation group as the direct product of the irreducible representations associated to the orbital angular momentum ℓ and the spins s_1 and s_2 of the two particles.

Every single-particle state $|\mathbf{p}, \sigma\rangle$ under the action of a rotation R transforms as

$$R|\mathbf{p}, \sigma\rangle = RU(\mathbf{p})|\mathbf{0}, \sigma\rangle = U(\mathbf{p}')U(\mathbf{p}')^{-1} RU(\mathbf{p})|\mathbf{0}, \sigma\rangle \ , \tag{A.17}$$

and $\mathbf{p}' = R\mathbf{p}$.[7] It is straightforward to show that

$$R = U(\mathbf{p}')^{-1} R U(\mathbf{p}) \ . \tag{A.18}$$

For that we explicitly write the Lorentz transformations $U(\mathbf{p}')$ and $U(\mathbf{p})$ as in Eq. (A.6) so that

$$U(\mathbf{p}')^{-1} R U(\mathbf{p}) = R(\hat{\mathbf{p}}') B_z(|\mathbf{p}|)^{-1} R(\hat{\mathbf{p}}')^{-1} R R(\hat{\mathbf{p}}) B_z(|\mathbf{p}|) R(\hat{\mathbf{p}})^{-1} \ . \tag{A.19}$$

Next, the product of rotations $R(\hat{\mathbf{p}}')^{-1} R R(\hat{\mathbf{p}})$ is a rotation around the z axis, $R_z(\gamma)$, since it leaves invariant $\hat{\mathbf{z}}$. Thus,

$$R(\hat{\mathbf{p}}')^{-1} R R(\hat{\mathbf{p}}) = R_z(\gamma) \ , \tag{A.20}$$

or, in other terms,

$$R(\hat{\mathbf{p}}') = R R(\hat{\mathbf{p}}) R_z(\gamma)^{-1} \ , \tag{A.21}$$

Taking into account Eqs. (A.20) and (A.21) in Eq. (A.19) it follows the result in Eq. (A.18) because $B_z(|\mathbf{p}|)$ and $R_z(\gamma)$ commute. Then Eq. (A.17) implies that

$$R|\mathbf{p}, \sigma\rangle = U(\mathbf{p}') R |\mathbf{0}, \sigma\rangle = \sum_{\sigma'} D^{(s)}(R)_{\sigma'\sigma} |\mathbf{p}', \sigma'\rangle \ , \tag{A.22}$$

with $D^{(s)}(R)$ the rotation matrix in the irreducible representation of the rotation group with spin s.

Now, we can use this result to find the action of the rotation R on the state $|\mathbf{p}, \sigma_1\sigma_2\rangle$ which is the direct product of the states $|\mathbf{p}, \sigma_1\rangle$ and $|-\mathbf{p}, \sigma_2\rangle$ (once the trivial CM movement is factorized out [56]). In this way,

$$R|\mathbf{p}, \sigma_1\sigma_2\rangle = \sum_{\sigma_1', \sigma_2'} D^{(s_1)}(R)_{\sigma_1'\sigma_1} D^{(s_2)}(R)_{\sigma_2'\sigma_2} |\mathbf{p}', \sigma_1'\sigma_2'\rangle \ . \tag{A.23}$$

[7] For a general Lorentz transformation these manipulations give rise to the Wigner rotation [56].

We are now ready to derive the action R on $|\ell m, \sigma_1\sigma_2\rangle$,

$$\begin{aligned} R|\ell m, \sigma_1\sigma_2\rangle &= \sum_{\sigma_1',\sigma_2'} D^{(s_1)}(R)_{\sigma_1'\sigma_1} D^{(s_2)}(R)_{\sigma_2'\sigma_2} \frac{1}{\sqrt{4\pi}} \int d\hat{\mathbf{p}}'\, Y_\ell^m(R^{-1}\hat{\mathbf{p}}')|\mathbf{p}', \sigma_1'\sigma_2'\rangle \\ &= \sum_{\sigma_1',\sigma_2',m'} D^{(\ell)}(R)_{m'm} D^{(s_1)}(R)_{\sigma_1'\sigma_1} D^{(s_2)}(R)_{\sigma_2'\sigma_2} |\ell m', \sigma_1'\sigma_2'\rangle \ . \end{aligned} \tag{A.24}$$

In this equation we have made use of the property of the spherical harmonics

$$Y_\ell^m(R^{-1}\hat{\mathbf{p}}') = \sum_{m'} D^{(\ell)}(R)_{m'm} Y_\ell^{m'}(\hat{\mathbf{p}}') \ . \tag{A.25}$$

Equation (A.24) shows that under rotation the states defined in Eq. (A.16) has the right transformation under the action of a rotation R, and our proposition above is shown to hold.

Now, because of the transformation in Eq. (A.24), corresponding to the direct product of spins s_1, s_2 and ℓ, we can combine these angular momentum indices and end with the LSJ basis. In the latter every state is labelled by the total angular momentum J, the third component of the total angular momentum μ, orbital angular momentum ℓ and total spin S (resulting from the composition of spins s_1 and s_2). Namely, we use the notation $|J\mu, \ell S\rangle$ for these states which are then given by

$$|J\mu, \ell S\rangle = \sum_{\sigma_1,\sigma_2,m,M} (\sigma_1\sigma_2 M|s_1 s_2 S)(mM\mu|\ell S J)|\ell m, \sigma_1\sigma_2\rangle \ , \tag{A.26}$$

where we have introduced the standard Clebsch-Gordan coefficients for the composition of two angular momenta.[8] Next we introduce the isospin indices α_1 and α_2 corresponding to the third components of the isospins τ_1 and τ_2. This does not modify any of our previous considerations since isospin does not transform under the action of spatial rotations. Within the isospin formalism the $\rho\rho$ states obey Bose-Einstein statistics and these symmetric states are defined by

$$|\mathbf{p}, \sigma_1\sigma_2, \alpha_1\alpha_2\rangle_S = \frac{1}{\sqrt{2}} \left(|\mathbf{p}, \sigma_1\sigma_2, \alpha_1\alpha_2\rangle + |-\mathbf{p}, \sigma_2\sigma_1, \alpha_2\alpha_1\rangle\right) \ , \tag{A.27}$$

with the subscript S indicating the symmetrized nature of the state under the exchange of the two particles. One can invert Eq. (A.16) and give the momentum-defined states in terms of those with well-defined orbital angular momentum,

$$\begin{aligned} |\mathbf{p}, \sigma_1\sigma_2, \alpha_1\alpha_2\rangle &= \sqrt{4\pi} \sum_{\ell,m} Y_\ell^m(\hat{\mathbf{p}})^* |\ell m, \sigma_1\sigma_2, \alpha_1\alpha_2\rangle \\ &= \sqrt{4\pi} \sum_{\substack{J,\mu,\ell,m \\ S,M,I,t_3}} Y_\ell^m(\hat{\mathbf{p}})^* (\sigma_1\sigma_2 M|s_1 s_2 S)(mM\mu|\ell S J)(\alpha_1\alpha_2 t_3|\tau_1\tau_2 I)|J\mu, \ell S, I t_3\rangle \ , \end{aligned} \tag{A.28}$$

with I the total isospin of the particle pair and t_3 is the third component. Taking into account this result we can write the symmetrized states as

$$|\mathbf{p}, \sigma_1\sigma_2, \alpha_1\alpha_2\rangle_S = \sqrt{4\pi} \sum_{\substack{J,\mu,\ell,m \\ S,M,I,t_3}} \frac{1+(-1)^{\ell+S+I}}{\sqrt{2}} (\sigma_1\sigma_2 M|s_1 s_2 S)(mM\mu|\ell S J)(\alpha_1\alpha_2 t_3|\tau_1\tau_2 I) Y_\ell^m(\hat{\mathbf{p}})^* |J\mu, \ell S, I t_3\rangle \ . \tag{A.29}$$

[8] The Clebsch-Gordan coefficient $(m_1 m_2 m_3|j_1 j_2 j_3)$ is the composition for $\mathbf{j}_1 + \mathbf{j}_2 = \mathbf{j}_3$, with m_i referring to the third components of the spins.

In deducing this expression we have taken into account the following symmetric properties of the Clebsch-Gordan coefficients

$$\begin{aligned}(\sigma_2\sigma_1 M|s_2s_1S) =&(-1)^{S-s_1-s_2}(\sigma_1\sigma_2 M|s_1s_2S)\ ,\\ (\alpha_2\alpha_1 t_3|t_2t_1I) =&(-1)^{I-t_1-t_2}(\alpha_1\alpha_2 t_3|\tau_1\tau_2 I)\ ,\\ Y_\ell^m(-\hat{\mathbf{p}}) =&(-1)^\ell Y_\ell^m(\hat{\mathbf{p}})\ .\end{aligned} \tag{A.30}$$

Of course, due to the fact that we are dealing with indistinguishable bosons within the isospin formalism it follows that $s_1 = s_2$, $\tau_1 = \tau_2$ as well as that $2\tau_1$ and $2s_1$ are even numbers. The combination $(1 + (-1)^{\ell+S+I})/\sqrt{2}$ in Eq. (A.29) is denoted in the following as $\chi(\ell ST)$ and takes into account the Bose-Einstein symmetric character of the two-particles, so that only states with even $\ell + S + I$ are allowed.

The inversion of Eq. (A.29) gives (we assume in the following that $\ell+S+I$ =even, so that $\chi(\ell ST) = \sqrt{2}$)

$$|J\mu,\ell S,It_3\rangle =\frac{1}{\sqrt{8\pi}}\sum_{\substack{\sigma_1,\,\sigma_2\\ M,\,m\\ \alpha_1,\,\alpha_2}}\int d\hat{\mathbf{p}}Y_\ell^m(\hat{\mathbf{p}})(\sigma_1\sigma_2 M|s_1s_2S)(mM\mu|\ell SJ)(\alpha_1\alpha_2 t_3|\tau_1\tau_2 I)|\mathbf{p},\sigma_1\sigma_2,\alpha_1\alpha_2\rangle_S\ . \tag{A.31}$$

We can also express the state $|J\mu,\ell S,It_3\rangle$ in terms of the states $|\mathbf{p},\sigma_1\sigma_2,\alpha_1\alpha_2\rangle$ without symmetrization by inverting Eq. (A.28). We would obtain the same expression as Eq. (A.31) but with a factor $1/\sqrt{4\pi}$ instead of $1/\sqrt{8\pi}$, namely,

$$|J\mu,\ell S,It_3\rangle =\frac{1}{\sqrt{4\pi}}\sum_{\substack{\sigma_1,\,\sigma_2\\ M,\,m\\ \alpha_1,\,\alpha_2}}\int d\hat{\mathbf{p}}Y_\ell^m(\hat{\mathbf{p}})(\sigma_1\sigma_2 M|s_1s_2S)(mM\mu|\ell SJ)(\alpha_1\alpha_2 t_3|\tau_1\tau_2 I)|\mathbf{p},\sigma_1\sigma_2,\alpha_1\alpha_2\rangle\ . \tag{A.32}$$

The extra factor of $1/\sqrt{2}$ in Eq. (A.31) is a symmetrization factor because of the Bose-Einstein symmetry properties of the two-particle state in the symmetrized states $|\mathbf{p},\sigma_1\sigma_2,\alpha_1\alpha_2\rangle_S$, which disappears when employing the nonsymmetrized states. In order to obtain the normalization of the states $|J\mu,\ell S,It_3\rangle$ it is indeed simpler to use Eq. (A.32) though, of course, the same result is obtained if starting from Eq. (A.31). The two-body particle states with definite three-momentum satisfy the normalization

$$\langle\mathbf{p}',\sigma_1'\sigma_2',\alpha_1'\alpha_2'|\mathbf{p},\sigma_1\sigma_2,\alpha_1\alpha_2\rangle =\frac{16\pi^2\sqrt{s}}{|\mathbf{p}|}\delta(\hat{\mathbf{p}}'-\hat{\mathbf{p}})\ , \tag{A.33}$$

The total energy conservation guarantees that the modulus of the final and initial three-momentum in Eq. (A.34) is the same, that we denote by $|\mathbf{p}|$. In terms of this result and Eq. (A.32) it follows straightforwardly by taking into account the orthogonal properties of Clebsch-Gordan coefficients and spherical harmonics that

$$\langle J'\mu',\ell'S',I't_3'|J\mu,\ell S,It_3\rangle =\frac{4\pi\sqrt{s}}{|\mathbf{p}|}\delta_{J'J}\delta_{\mu'\mu}\delta_{\ell'\ell}\delta_{S'S}\delta_{I'I}\delta_{t_3't_3} \tag{A.34}$$

We are interested in the partial-wave amplitude corresponding to the transition between states with quantum numbers $J\bar{\ell}\bar{S}I$ to states $J\ell SI$, that corresponds to the matrix element

$$T^{(JI)}_{\ell S;\bar{\ell}\bar{S}} =\langle J\mu,\ell S,It_3|\hat{T}|J\mu,\bar{\ell}\bar{S},It_3\rangle\ , \tag{A.35}$$

with $\hat{T}$ the T-matrix scattering operator. Here we take the convention that the quantum numbers referring to the initial state are barred. Of course, the matrix element in Eq. (A.35) is independent of μ and t_3 because of invariance under rotations in ordinary and isospin spaces, respectively. We can calculate this scattering matrix element in terms of those in the basis with definite three-momentum by replacing in Eq. (A.35) the states in the $J\ell S$ basis as given in Eq. (A.31). We then obtain in a first step

$$T^{(JI)}_{\ell S;\bar{\ell}\bar{S}} = \frac{1}{8\pi}\sum \int d\hat{\mathbf{p}} \int d\hat{\mathbf{p}}'\, Y^m_\ell(\hat{\mathbf{p}}')^* Y^{\bar{m}}_{\bar{\ell}}(\hat{\mathbf{p}})(\sigma_1\sigma_2 M|s_1 s_2 S)(mM\mu|\ell S J)(\alpha_1\alpha_2 t_3|\tau_1\tau_2 I)$$
$$\times(\bar{\sigma}_1\bar{\sigma}_2\bar{M}|\bar{s}_1\bar{s}_2 S)(\bar{m}\bar{M}\mu|\bar{\ell}\bar{S}J)(\bar{\alpha}_1\bar{\alpha}_2 t_3|\bar{\tau}_1\bar{\tau}_2 I)_S\langle \mathbf{p}', \sigma_1\sigma_2, \alpha_1\alpha_2|\hat{T}|\mathbf{p}, \bar{\sigma}_1\bar{\sigma}_2, \bar{\alpha}_1\bar{\alpha}_2\rangle_S \ , \tag{A.36}$$

Here we have not shown the explicit indices over which the sum is done in order not to overload the notation.[9] We use next the rotation invariance of the T-matrix operator $\hat{T}$ to simplify the previous integral so that, at the end, we have just the integration over the final three-momentum angular solid. There are several steps involved that we give in quite detail. The referred rotational invariance of $\hat{T}$ implies that it remains invariant under the transformation $\hat{T} \to R(\hat{\mathbf{p}})\hat{T}R(\hat{\mathbf{p}})^\dagger$, which implies at the level of the matrix elements that

$${}_S\langle \mathbf{p}', \sigma_1\sigma_2, \alpha_1\alpha_2|\hat{T}|\mathbf{p}, \bar{\sigma}_1\bar{\sigma}_2, \bar{\alpha}_1\bar{\alpha}_2\rangle_S = {}_S\langle \mathbf{p}', \sigma_1\sigma_2, \alpha_1\alpha_2|R(\hat{\mathbf{p}})\hat{T}R(\hat{\mathbf{p}})^\dagger|\mathbf{p}, \bar{\sigma}_1\bar{\sigma}_2, \bar{\alpha}_1\bar{\alpha}_2\rangle_S \ . \tag{A.37}$$

Under the action of the rotation $R(\hat{\mathbf{p}})^\dagger$ ($R(\hat{\mathbf{p}})^\dagger\hat{\mathbf{p}} = \hat{\mathbf{z}}$ and $R(\hat{\mathbf{p}})^\dagger\hat{\mathbf{p}}' = \hat{\mathbf{p}}''$) the final and initial states transform as, cf. Eq. (A.23),

$$R(\hat{\mathbf{p}})^\dagger|\mathbf{p}, \bar{\sigma}_1\bar{\sigma}_2, \bar{\alpha}_1\bar{\alpha}_2\rangle_S = \sum_{\bar{\sigma}'_1,\bar{\sigma}'_2} D^{(\bar{s}_1)}_{\bar{\sigma}'_1\bar{\sigma}_1}(R^\dagger) D^{(\bar{s}_2)}_{\bar{\sigma}'_2\bar{\sigma}_2}(R^\dagger)|\hat{\mathbf{z}}, \bar{\sigma}'_1\bar{\sigma}'_2, \bar{\alpha}_1\bar{\alpha}_2\rangle_S \ ,$$
$$R(\hat{\mathbf{p}})^\dagger|\mathbf{p}', \sigma_1\sigma_2, \alpha_1\alpha_2\rangle_S = \sum_{\sigma'_1,\sigma'_2} D^{(s_1)}_{\sigma'_1\sigma_1}(R^\dagger) D^{(s_2)}_{\sigma'_2\sigma_2}(R^\dagger)|\hat{\mathbf{p}}'', \sigma'_1\sigma'_2, \alpha_1\alpha_2\rangle_S \ , \tag{A.38}$$

with the convention that R inside the argument of the rotation matrices refers to $R(\hat{\mathbf{p}})$. We insert Eqs. (A.37) and (A.38) into Eq. (A.36), and next transform $\hat{\mathbf{p}}' \to \hat{\mathbf{p}}''$ as integrations variables, take into account the invariance of the solid angle measure under such rotation and use Eq. (A.25) for

$$Y^{\bar{m}}_{\bar{\ell}}(\hat{\mathbf{p}}) = Y^{\bar{m}}_{\bar{\ell}}(R(\hat{\mathbf{p}})\hat{\mathbf{z}}) = \sum_{\bar{m}'} D^{(\bar{\ell})}_{\bar{m}'\bar{m}}(R^\dagger) Y^{\bar{m}'}_{\bar{\ell}}(\hat{\mathbf{z}}) \ ,$$
$$Y^m_\ell(\hat{\mathbf{p}}') = Y^m_\ell(R(\hat{\mathbf{p}})\hat{\mathbf{p}}'') = \sum_{m'} D^{(\ell)}_{m'm}(R^\dagger) Y^{m'}_\ell(\hat{\mathbf{p}}'') \ . \tag{A.39}$$

Then, Eq. (A.36) for $T^{(JI)}_{\ell S;\bar{\ell}\bar{S}}$ can be rewritten as

$$T^{(JI)}_{\ell S;\bar{\ell}\bar{S}} = \frac{1}{8\pi}\sum \int d\hat{\mathbf{p}} \int d\hat{\mathbf{p}}''(\sigma_1\sigma_2 M|s_1 s_2 S)(mM\mu|\ell S J)(\alpha_1\alpha_2 t_3|\tau_1\tau_2 I) D^{(s_1)}_{\sigma'_1\sigma_1}(R^\dagger)^* D^{(s_2)}_{\sigma'_2\sigma_2}(R^\dagger)^*$$
$$\times D^{(\ell)}_{m'm}(R^\dagger)^* Y^{m'}_\ell(\hat{\mathbf{p}}'')^*(\bar{\sigma}_1\bar{\sigma}_2\bar{M}|\bar{s}_1\bar{s}_2\bar{S})(\bar{m}\bar{M}\mu|\bar{\ell}\bar{S}J)(\bar{\alpha}_1\bar{\alpha}_2 t_3|\bar{\tau}_1\bar{\tau}_2 I)$$
$$\times D^{(\bar{s}_1)}_{\bar{\sigma}'_1\bar{\sigma}_1}(R^\dagger) D^{(\bar{s}_2)}_{\bar{\sigma}'_2\bar{\sigma}_2}(R^\dagger) D^{(\bar{\ell})}_{\bar{m}'\bar{m}}(R^\dagger) Y^{\bar{m}'}_{\bar{\ell}}(\hat{\mathbf{z}})_S\langle \mathbf{p}'', \sigma'_1\sigma'_2, \alpha_1\alpha_2|\hat{T}|\,|\mathbf{p}|\hat{\mathbf{z}}, \bar{\sigma}'_1\bar{\sigma}'_2, \bar{\alpha}_1\bar{\alpha}_2\rangle_S \ . \tag{A.40}$$

Let us recall that from the composition of two rotation matrices one has that [56, 57]

$$\sum_{m_1,m_2}(m_1 m_2 M|\ell_1\ell_2 L) D^{(\ell_1)}_{m'_1 m_1}(R) D^{(\ell_2)}_{m'_2 m_2}(R) = \sum_{M'}(m'_1 m'_2 M'|\ell_1\ell_2 L) D^{(L)}_{M'M}(R) \ . \tag{A.41}$$

[9] They correspond to those indicated under the summation symbol in Eq. (A.31) both for the initial and final states.

We apply this result first to two combinations in Eq. (A.40):

$$\sum_{\sigma_1,\sigma_2}(\sigma_1\sigma_2 M|s_1s_2S)D^{(s_1)}_{\sigma_1'\sigma_1}(R^\dagger)D^{(s_2)}_{\sigma_2'\sigma_2}(R^\dagger)=\sum_{M'}(\sigma_1'\sigma_2'M'|s_1s_2S)D^{(S)}_{M'M}(R^\dagger)$$
$$\sum_{\bar\sigma_1,\bar\sigma_2}(\bar\sigma_1\bar\sigma_2\bar M|\bar s_1\bar s_2\bar S)D^{(\bar s_1)}_{\bar\sigma_1'\bar\sigma_1}(R^\dagger)D^{(\bar s_2)}_{\bar\sigma_2'\bar\sigma_2}(R^\dagger)=\sum_{\bar M'}(\bar\sigma_1'\bar\sigma_2'\bar M'|\bar s_1\bar s_2\bar S)D^{(\bar S)}_{\bar M'\bar M}(R^\dagger)\ , \tag{A.42}$$

so that Eq. (A.40) becomes

$$\begin{aligned}T^{(JI)}_{\ell S;\bar\ell\bar S}=&\frac{1}{8\pi}\sum\int d\hat{\mathbf{p}}\int d\hat{\mathbf{p}}''(\sigma_1'\sigma_2'M'|s_1s_2S)D^{(S)}_{M'M}(R^\dagger)^*D^{(\ell)}_{m'm}(R^\dagger)^*(mM\mu|\ell SJ)(\alpha_1\alpha_2t_3|\tau_1\tau_2I)Y^{m'}_\ell(\hat{\mathbf{p}}'')^*\\&\times(\bar\sigma_1'\bar\sigma_2'\bar M'|\bar s_1\bar s_2\bar S)D^{(\bar S)}_{\bar M'\bar M}(R^\dagger)D^{(\bar\ell)}_{\bar m'\bar m}(R^\dagger)(\bar m\bar M\mu|\bar\ell\bar SJ)(\bar\alpha_1\bar\alpha_2t_3|\bar\tau_1\bar\tau_2I)Y^{\bar m'}_{\bar\ell}(\hat{\mathbf{z}})\\&\times{}_S\langle\mathbf{p}'',\sigma_1'\sigma_2',\alpha_1\alpha_2|\hat T|\,|\mathbf{p}|\hat{\mathbf{z}},\bar\sigma_1'\bar\sigma_2',\bar\alpha_1\bar\alpha_2\rangle_S\ .\end{aligned} \tag{A.43}$$

The same relation in Eq. (A.41) is applied once more to the following combinations in Eq. (A.43):

$$\sum_{m,M}(mM\mu|\ell SJ)D^{(S)}_{M'M}(R^\dagger)D^{(\ell)}_{m'm}(R^\dagger)=\sum_{\mu'}(m'M'\mu'|\ell SJ)D^{(J)}_{\mu'\mu}(R^\dagger)\ ,$$
$$\sum_{\bar m,\bar M}(\bar m\bar M\mu|\bar\ell\bar SJ)D^{(\bar S)}_{\bar M'\bar M}(R^\dagger)D^{(\bar\ell)}_{\bar m'\bar m}(R^\dagger)=\sum_{\bar\mu'}(\bar m'\bar M'\bar\mu'|\bar\ell\bar SJ)D^{(J)}_{\bar\mu'\mu}(R^\dagger)\ . \tag{A.44}$$

We take Eq. (A.44) into Eq. (A.43) which now reads

$$\begin{aligned}T^{(JI)}_{\ell S;\bar\ell\bar S}=&\frac{1}{8\pi}\sum\int d\hat{\mathbf{p}}\int d\hat{\mathbf{p}}''(\sigma_1'\sigma_2'M'|s_1s_2S)(m'M'\mu'|\ell SJ)(\alpha_1\alpha_2t_3|\tau_1\tau_2I)Y^{m'}_\ell(\hat{\mathbf{p}}'')^*\\&\times(\bar\sigma_1'\bar\sigma_2'\bar M'|\bar s_1\bar s_2\bar S)(\bar m'\bar M'\bar\mu'|\bar\ell\bar SJ)(\bar\alpha_1\bar\alpha_2t_3|\bar\tau_1\bar\tau_2I)Y^{\bar m'}_{\bar\ell}(\hat{\mathbf{z}})D^{(J)}_{\mu'\mu}(R^\dagger)^*D^{(J)}_{\bar\mu'\mu}(R^\dagger)\\&\times{}_S\langle\mathbf{p}'',\sigma_1'\sigma_2',\alpha_1\alpha_2|\hat T|\,|\mathbf{p}|\hat{\mathbf{z}},\bar\sigma_1'\bar\sigma_2',\bar\alpha_1\bar\alpha_2\rangle_S\end{aligned} \tag{A.45}$$

Now, the partial wave amplitude $T^{(JI)}_{\ell S;\bar\ell\bar S}$ is independent of μ so that we have that

$$T^{(JI)}_{\ell S;\bar\ell\bar S}=\frac{1}{2J+1}\sum_{\mu=-J}^{J}T^{(JI)}_{\ell S;\bar\ell\bar S}\ . \tag{A.46}$$

The same result in Eq. (A.45) is obtained with the product $D^{(J)}_{\mu'\mu}(R^\dagger)^*D^{(J)}_{\bar\mu'\mu}(R^\dagger)$ replaced by

$$\frac{1}{2J+1}\sum_{\mu=-J}^{J}D^{(J)}_{\mu'\mu}(R^\dagger)^*D^{(J)}_{\bar\mu'\mu}(R^\dagger)=\frac{\delta_{\bar\mu'\mu'}}{2J+1}\ , \tag{A.47}$$

as follows from the unitarity character of the rotation matrices. As a consequence any dependence in $\hat{\mathbf{p}}$ present in the integrand of Eq. (A.45) disappears in the average of Eq. (A.46), the integration in the solid angle $\hat{\mathbf{p}}$ is trivial and it gives a factor 4π. Taking into account the Kronecker delta from Eq. (A.47) in the third component of the total angular momentum and a new one that arises because $Y^{\bar m'}_{\bar\ell}(\hat{\mathbf{z}})$ is not zero only for $\bar m'=0$, we then end with the following expression for $T^{(JI)}_{\ell S;\bar\ell\bar S}$:

$$\begin{aligned}T^{(JI)}_{\ell S;\bar\ell\bar S}=\frac{Y^0_{\bar\ell}(\hat{\mathbf{z}})}{2(2J+1)}\sum_{\substack{\sigma_1,\sigma_2,\bar\sigma_1\\\bar\sigma_2,\alpha_1,\alpha_2\\\bar\alpha_1,\bar\alpha_2,m}}&\int d\hat{\mathbf{p}}''\,Y^m_\ell(\hat{\mathbf{p}}'')^*(\sigma_1\sigma_2M|s_1s_2S)(mM\bar M|\ell SJ)(\bar\sigma_1\bar\sigma_2\bar M|\bar s_1\bar s_2\bar S)(0\bar M\bar M|\bar\ell\bar SJ)\\&\times(\alpha_1\alpha_2t_3|\tau_1\tau_2I)(\bar\alpha_1\bar\alpha_2t_3|\bar\tau_1\bar\tau_2I)_S\langle\mathbf{p}'',\sigma_1\sigma_2,\alpha_1\alpha_2|\hat T|\,|\mathbf{p}|\hat{\mathbf{z}},\bar\sigma_1\bar\sigma_2,\bar\alpha_1\bar\alpha_2\rangle_S\ ,\end{aligned} \tag{A.48}$$

where we have removed the primes on top of the spin and orbital angular momentum third-component symbols and in the previous sum $M = \sigma_1 + \sigma_2$ and $\bar{M} = \bar{\sigma}_1 + \bar{\sigma}_2$.

Next, we derive the unitarity relation corresponding to our normalization for the partial-wave projected amplitudes $T^{(JI)}_{\ell S;\bar{\ell}\bar{S}}$. We write the $\hat{S}$ matrix as

$$\hat{S} = I - i\hat{T} \tag{A.49}$$

which satisfies the standard unitarity relation

$$\hat{S} \cdot \hat{S}^\dagger = \mathbb{I} \ , \tag{A.50}$$

with $\mathbb{I}$ the identity matrix. In terms of the T-matrix, cf. (A.49), this implies that

$$\hat{T} - \hat{T}^\dagger = -i\hat{T}\hat{T}^\dagger \ . \tag{A.51}$$

Expressed with the matrix elements in the basis ℓSJ this relation becomes

$$2\mathrm{Im}\hat{T}^{(JI)}_{\ell S;\bar{\ell}\bar{S}} = -\langle J\mu, \ell S, Tt_3|\hat{T}\hat{T}^\dagger|J\mu, \bar{\ell}\bar{S}, Tt_3\rangle \ . \tag{A.52}$$

In deriving the left-hand side of this equation we have taken into account that because of time-reversal symmetry $T^{(JI)}_{\ell S;\bar{\ell}\bar{S}} = T^{(JI)}_{\bar{\ell}\bar{S};\ell S}$. On the right-hand side we introduce now a two-body resolution of the identity of states $|J\mu, \ell S, It_3\rangle$ (we have restricted our vector space to the one generated by these states) such that, taking into account their normalization in Eq. (A.34), one ends with

$$\mathrm{Im}T^{(JI)}_{\ell S;\bar{\ell}\bar{S}} = -\sum_{\ell'', S''} \frac{|\mathbf{p}''|}{8\pi\sqrt{s}} T^{(JI)}_{\ell,S;\ell'',S''} T^{(JI)*}_{\ell'',S'';\bar{\ell}\bar{S}} \ . \tag{A.53}$$

The phase space factor is included in the diagonal matrix

$$\rho_{ij} = \frac{|\mathbf{p}|_i}{8\pi\sqrt{s}}\delta_{ij} \ . \tag{A.54}$$

A more standard definition of the S-matrix implies to redefine it as

$$\hat{S} \to S = 2\rho^{\frac{1}{2}}\hat{S}\rho^{\frac{1}{2}} = I - 2i\rho^{\frac{1}{2}}\hat{T}\rho^{\frac{1}{2}} \ , \tag{A.55}$$

such that now the diagonal matrix elements of the identity operator I and S are just 1 and $\eta_i e^{2i\delta_i}$, in order, where η_i is the inelasticity for channel i and δ_i its phase shift.

References

[1] R. H. Dalitz and S. F. Tuan, Phys. Rev. Lett. **2** (1959) 425.

[2] J. A. Oller and U.-G. Meißner, Phys. Lett. B **500**, 263 (2001) [hep-ph/0011146].

[3] D. Jido, J. A. Oller, E. Oset, A. Ramos and U.-G. Meißner, Nucl. Phys. A **725**, 181 (2003) [nucl-th/0303062].

[4] H. Y. Lu *et al.* [CLAS Collaboration], Phys. Rev. C **88**, 045202 (2013) [arXiv:1307.4411].

[5] C. Patrignani *et al.* (Particle Data Group), Chin Phys. C **40**, 100001 (2016).

[6] J. D. Weinstein and N. Isgur, Phys. Rev. D **41**, 2236 (1990).

[7] G. Janssen, B. C. Pearce, K. Holinde and J. Speth, Phys. Rev. D **52**, 2690 (1995) [nucl-th/9411021].

[8] J. A. Oller and E. Oset, Nucl. Phys. A **620**, 438 (1997); (E) Nucl. Phys. A **652**, 407 (1999) [hep-ph/9702314].

[9] R. Molina, D. Nicmorus and E. Oset, Phys. Rev. D **78**, 114018 (2008) [arXiv:0809.2233 [hep-ph]].

[10] L. S. Geng and E. Oset, Phys. Rev. D **79** (2009) 074009 [arXiv:0812.1199 [hep-ph]].

[11] H. Nagahiro, J. Yamagata-Sekihara, E. Oset, S. Hirenzaki and R. Molina, Phys. Rev. D **79**, 114023 (2009) [arXiv:0809.3717 [hep-ph]]; J. J. Xie, E. Oset and L. S. Geng, Phys. Rev. C **93**, 025202 (2016) [arXiv:1509.06469 [nucl-th]].

[12] E. Oset, L. S. Geng and R. Molina, J. Phys. Conf. Ser. **348** (2012) 012004;

[13] D. B. Lichtenberg, *Unitary Symmetry and Elementary Particles*, 2nd edition, Academic Press, New York, 1978.

[14] M. Koll, R. Ricken, D. Merten, B. C. Metsch and H. R. Petry, Eur. Phys. J. A **9**, 73 (2000) [hep-ph/0008220].

[15] R. Ricken, M. Koll, D. Merten, B. C. Metsch and H. R. Petry, Eur. Phys. J. A **9**, 221 (2000) [hep-ph/0008221].

[16] Review on 'Quark Model' in PDG(2016) [5] by C. Amsler, T. DeGrand and B. Krusche.

[17] M. Krammer and H. Krasemann, Phys. Lett. B **73**, 58 (1978).

[18] Z. P. Li, F. E. Close and T. Barnes, Phys. Rev. D **43**, 2161 (1991).

[19] L. Y. Dai and M. R. Pennington, Phys. Rev. D **90**, no. 3, 036004 (2014) [arXiv:1404.7524 [hep-ph]].

[20] T. Mori *et al.* [Belle Collaboration], Phys. Rev. D **75**, 051101 (2007) [hep-ex/0610038]; J. Phys. Soc. Jap. **76**, 074102 (2007) [arXiv:0704.3538 [hep-ex]].

[21] K. Abe *et al.* [Belle Collaboration], arXiv:0711.1926 [hep-ex]; S. Uehara *et al.* [Belle Collaboration], Phys. Rev. D **78**, 052004 (2008) [arXiv:0805.3387 [hep-ex]]; S. Uehara *et al.* [Belle Collaboration], Phys. Rev. D **79**, 052009 (2009) [arXiv:0903.3697 [hep-ex]].

[22] J. A. Carrasco, J. Nebreda, J. R. Pelaez and A. P. Szczepaniak, Phys. Lett. B **749**, 399 (2015) [arXiv:1504.03248 [hep-ph]]; J. T. Londergan, J. Nebreda, J. R. Pelaez and A. Szczepaniak, Phys. Lett. B **729**, 9 (2014) [arXiv:1311.7552 [hep-ph]]; J. R. Pelaez and F. J. Yndurain, Phys. Rev. D **69**, 114001 (2004) [hep-ph/0312187]; R. Garcia-Martin, R. Kaminski, J. R. Pelaez, J. Ruiz de Elvira and F. J. Yndurain, Phys. Rev. D **83**, 074004 (2011) [arXiv:1102.2183 [hep-ph]].

[23] A. V. Anisovich, V. V. Anisovich and A. V. Sarantsev, Phys. Rev. D **62**, 051502 (2000) [hep-ph/0003113].

[24] B. Ananthanarayan, G. Colangelo, J. Gasser and H. Leutwyler, Phys. Rept. **353**, 207 (2001) [hep-ph/0005297].

[25] G. Veneziano, Nuovo Cim. **57**, 190 (1968); C. Lovelace, Phys. Lett. B **28**, 264 (1968); J. A. Saphiro, Phys. Rev. **179**, 1345 (1969).

[26] U.-G. Meißner, Phys. Rept. **161** (1988) 213.

[27] M. Bando, T. Kugo, S. Uehara, K. Yamawaki and T. Yanagida, Phys. Rev. Lett. **54**, 1215 (1985).

[28] M. Bando, T. Kugo and K. Yamawaki, Phys. Rept. **164**, 217 (1988).

[29] J. A. Oller and E. Oset, Phys. Rev. D **60**, 074023 (1999) [hep-ph/9809337].

[30] N. Kaiser, P. B. Siegel and W. Weise, Nucl. Phys. A **594** (1995) 325 [nucl-th/9505043]; N. Kaiser, P. B. Siegel and W. Weise, Phys. Lett. B **362** (1995) 23 [nucl-th/9507036].

[31] Z. H. Guo, J. A. Oller and J. Ruiz de Elvira, Phys. Rev. D **86**, 054006 (2012) [arXiv:1206.4163 [hep-ph]].

[32] L. Roca, E. Oset and J. Singh, Phys. Rev. D **72**, 014002 (2005) [hep-ph/0503273].

[33] L. Alvarez-Ruso, J. A. Oller and J. M. Alarcon, Phys. Rev. D **80**, 054011 (2009) [arXiv:0906.0222 [hep-ph]]; Phys. Rev. D **82**, 094028 (2010) [arXiv:1007.4512 [hep-ph]].

[34] S. Sarkar, E. Oset and M. J. Vicente Vacas, Nucl. Phys. A **750**, 294 (2005) Erratum: [Nucl. Phys. A **780**, 90 (2006)] [nucl-th/0407025].

[35] J. A. Oller, Nucl. Phys. A **725**, 85 (2003).

[36] J. A. Oller, Phys. Lett. B **477**, 187 (2000) [hep-ph/9908493].

[37] J. A. Oller, Phys. Lett. B **477**, 187 (2000) [hep-ph/9908493] R. L. Delgado, A. Dobado and F. J. Llanes-Estrada, Phys. Rev. Lett. **114**, 221803 (2015) [arXiv:1408.1193 [hep-ph]]; A. Dobado, M. J. Herrero, J. R. Pelaez and E. Ruiz Morales, Phys. Rev. D **62**, 055011 (2000) [hep-ph/9912224].

[38] U.-G. Meißner and J. A. Oller, Nucl. Phys. A **673**, 311 (2000) [nucl-th/9912026]; J. M. Alarcon, J. Martin Camalich and J. A. Oller, Annals Phys. **336**, 413 (2013) [arXiv:1210.4450 [hep-ph]].

[39] M. Albaladejo, J. A. Oller and L. Roca, Phys. Rev. D **82**, 094019 (2010) [arXiv:1011.1434 [hep-ph]].

[40] P. C. Bruns, M. Mai and U.-G. Meißner, Phys. Lett. B **697** (2011) 254 [arXiv:1012.2233 [nucl-th]]. M. Mai and U.-G. Meißner, Eur. Phys. J. A **51** (2015) no.3, 30 [arXiv:1411.7884 [hep-ph]].

[41] D. Gamermann and E. Oset, Eur. Phys. J. A **33**, 119 (2007) [arXiv:0704.2314 [hep-ph]].

[42] J. M. Dias, F. Aceti and E. Oset, Phys. Rev. D **91**, no. 7, 076001 (2015) [arXiv:1410.1785 [hep-ph]].

[43] O. Romanets, L. Tolos, C. Garcia-Recio, J. Nieves, L. L. Salcedo and R. G. E. Timmermans, Phys. Rev. D **85**, 114032 (2012) [arXiv:1202.2239 [hep-ph]].

[44] X. W. Kang and J. A. Oller, Phys. Rev. D **94**, no. 5, 054010 (2016) [arXiv:1606.06665 [hep-ph]].

[45]

[45] L. Roca, M. Mai, E. Oset and U.-G. Meißner, Eur. Phys. J. C **75** (2015) no.5, 218 [arXiv:1503.02936 [hep-ph]].

[46] J. A. Oller, E. Oset and J. R. Pelaez, Phys. Rev. D **59**, 074001 (1999); (E) Phys. Rev. D **60**, 099906 (1999); (E) Phys. Rev. D **75**, 099903 (2007). [hep-ph/9804209].

[47] T. Hyodo, D. Jido and A. Hosaka, Phys. Rev. C **85**, 015201 (2012) [arXiv:1108.5524 [nucl-th]].

[48] F. Aceti and E. Oset, Phys. Rev. D **86**, 014012 (2012) [arXiv:1202.4607 [hep-ph]].

[49] T. Sekihara, T. Hyodo and D. Jido, PTEP **2015**, 063D04 (2015) [arXiv:1411.2308 [hep-ph]].

[50] M. Albaladejo and J. A. Oller, Phys. Rev. Lett. **101**, 252002 (2008) [arXiv:0801.4929 [hep-ph]].

[51] D. V. Bugg, Eur. Phys. J. C **52**, 55 (2007) [arXiv:0706.1341 [hep-ex]].

[52] M. Albaladejo and J. A. Oller, Phys. Rev. C **84**, 054009 (2011) [arXiv:1107.3035 [nucl-th]]; *ibid* **86** 034005 (2012) [arXiv:1201.0443 [nucl-th]].

[53] Z. H. Guo, J. A. Oller and G. Ríos, Phys. Rev. C **89**, no. 1, 014002 (2014) [arXiv:1305.5790 [nucl-th]]; J. A. Oller, Phys. Rev. C **93**, 024002 (2016) [arXiv:1402.2449 [nucl-th]]; D. R. Entem and J. A. Oller, arXiv:1610.01040 [nucl-th].

[54] G.F. Chew and S. Mandelstam, Phys. Rev. **119** (1960) 467.

[55] M. Albaladejo and J. A. Oller, Phys. Rev. C **84**, 054009 (2011) [arXiv:1107.3035 [nucl-th]]; *ibid* **86**, 034005 (2012) [arXiv:1201.0443 [nucl-th]]; J. A. Oller, Phys. Rev. C **93**, 024002 (2016) [arXiv:1402.2449 [nucl-th]].

[56] A. D. Martin and T. D. Spearman, *Elementary Particle Theory*, Noth-Holland Publishing Company, Amsterdam, 1970.

[57] M. E. Rose, *Elementary Theory of Angular Momentum*, Dover, New York, 1995.